Solar Physics
DOI: 10.1007/•••••-•••-•••-••••-•

Twisted Flux Tube Emergence Evidenced in Longitudinal Magnetograms: Magnetic Tongues

M.L. Luoni · P. Démoulin · C.H. Mandrini · L. van Driel-Gesztelyi

Abstract Bipolar active regions (ARs) are thought to be formed by twisted flux tubes, as the presence of such twist is theoretically required for a cohesive rise through the whole convective zone. We use longitudinal magnetograms to demonstrate that a clear signature of a global magnetic twist is present, particularly, during the emergence phase when the AR is forming in a much weaker pre-existing magnetic field environment. The twist is characterised by the presence of elongated polarities, called "magnetic tongues", which originate from the azimuthal magnetic field component. The tongues first extend in size before retracting when the maximum magnetic flux is reached. This implies an apparent rotation of the magnetic bipole. Using a simple half-torus model of an emerging twisted flux tube having a uniform twist profile, we derive how the direction of the polarity inversion line and the elongation of the tongues depend on the global twist in the flux rope. Using a sample of 40 ARs, we verify that the helicity sign, determined from the magnetic polarity distribution pattern, is consistent with the sign derived from the photospheric helicity flux computed from magnetogram time series, as well as from other proxies such as sheared coronal loops, sigmoids,

M.L. Luoni · C.H. Mandrini
Instituto de Astronomía y Física del Espacio,
CONICET-UBA, CC. 67, Suc. 28, 1428 Buenos Aires,
Argentina email: mluoni@iafe.uba.ar

C.H. Mandrini
Facultad de Ciencias Exactas y Naturales, FCEN-UBA,
Buenos Aires, Argentina

P. Démoulin · L. van Driel-Gesztelyi
Observatoire de Paris, LESIA, UMR8109 (CNRS), F-92195,
Meudon Principal Cedex, France

L. van Driel-Gesztelyi
UCL - Mullard Space Science Laboratory, Holmbury St.
Mary, Dorking, Surrey, RH5 6NT, U.K.

L. van Driel-Gesztelyi
Konkoly Observatory of the Hungarian Academy of Sciences,
Budapest, Hungary

flare ribbons and/or the associated magnetic cloud observed *in situ* at 1 AU. The evolution of the tongues observed in emerging ARs is also closely similar to the evolution found in recent MHD numerical simulations. We also found that the elongation of the tongue formed by the leading magnetic polarity is significantly larger than that of the following polarity. This newly discovered asymmetry is consistent with an asymmetric Ω-loop emergence, trailing the solar rotation, which was proposed earlier to explain other asymmetries in bipolar ARs.

Keywords: Active Regions, Magnetic Fields; Corona, Structures; Helicity, Magnetic; Helicity, Observations

1. Introduction

Magnetic activity on the Sun is widely thought to have its origin in the dynamo located just below the base of the convective zone (CZ), in the tachocline. At some point during the amplification of the magnetic field, a flux tube is supposed to become buoyantly unstable and, then, it starts crossing the CZ. The flux tube needs to be sufficiently twisted to be able to survive its travel through the CZ (Emonet and Moreno-Insertis, 1998; Cheung, Moreno-Insertis, and Schüssler, 2006). However, in order that the twisted flux tube, or flux rope, to show a tilt direction consistent with observations (Joy's law), the initial twist needs to be less than half of that needed for a cohesive rise (Fan, 2008). Rising flux ropes are also affected by the large-scale convective motions (Jouve and Brun, 2009).

The global MHD simulations of flux ropes in the CZ (see references in the previous paragraph) typically end around 10-20 Mm below the photosphere, where a sharp stratification of the plasma is present together with a change of the physical regime. Local MHD simulations calculate the flux rope evolution from below the photosphere to the low corona (within a range of altitudes, typically from ≈ -5 Mm to 10 Mm, the origin of heights being at the bottom of the photosphere). The crossing of the photosphere by a flux tube is difficult for several reasons, first, the flux tube is no longer buoyant, second, there is a change of regime (from high to low plasma β, with β being the ratio between the plasma and the magnetic pressure), and finally, it has a much larger radius than the local gravitational scale height. The flux tube flattens below the photosphere forming a horizontal layer and, later, its upper part eventually succeeds to cross the photosphere when the accumulating magnetic field becomes strong enough to be buoyant again (*e.g.*, Magara, 2001; Archontis *et al.*, 2004; Magara, 2004; Manchester *et al.*, 2004; Murray *et al.*, 2006). However, magnetic dips which are inevitably present in a twisted flux tube are loaded with dense material, so that the tube becomes gravitationally anchored to the photosphere in the absence of magnetic reconnection (Pariat *et al.*, 2004).

The MHD simulations, discussed above, start with a horizontal flux rope located significantly below the photosphere. A density or a velocity perturbation, with a Gaussian spatial shape along the tube, induces the buoyant instability and the portion of the flux rope which is arching upward starts to emerge across the photosphere. However, the inclination of the axis is typically not strong enough

to allow the evacuation of the dense plasma in the flux rope legs and only its upper part is able to cross the photosphere. This problem is solved by starting the simulation with an already upward arching flux rope. For field strengths large enough, the axis of the toroidal loop emerges fully into the corona (Hood *et al.*, 2009; MacTaggart and Hood, 2009). This simulation of flux emergence gives a photospheric field distribution closer to the observed active region (AR) magnetograms (if rescaled to a typical AR size, but it also implies a thicker photosphere). Moreover, unlike the results obtained with an initially straight flux tube, the separation of the magnetic field polarities does not continue indefinitely with time, but has a finite maximum value, as observed.

In observations, the emergence of an isolated AR is typically detected at the photospheric level by the growth and separation of two opposite magnetic polarities. When viewed at high spatial resolution, it is seen that the magnetic flux tube splits in many nearly parallel thin strands that emerge successively (Zwaan, 1985; Strous *et al.*, 1996; Pariat *et al.*, 2004). Nevertheless, the global coherence of photospheric motions indicates the presence of one main coherent progenitor flux tube. The emergence of isolated ARs is more appropriate to study the intrinsic properties of emerging flux tubes, since due to the lack of interaction with pre-existing fields it shows their characteristics more clearly.

Signatures of twisted magnetic flux emergence besides the growth and polarity separation also include a rotation of the bipole (*i.e.* a change of direction of the line joining the flux-weighted center of both magnetic polarities). Though the polarities in some ARs show a genuine physical long-term relative rotation, which is interpreted as the emergence of a writhed flux tube (see López Fuentes *et al.*, 2003), in most cases a rotation observed during the short flux emergence period is not a true rotation of the magnetic field configuration. The apparent rotation of the bipole is a consequence of the evolution of the so-called "magnetic tongues", which are extensions of the approximately round magnetic field polarities expected for a twisted emerging bipolar field (see Figure 1 and López Fuentes *et al.*, 2000). Magnetic tongues which resemble the *yin yang* pattern, can be understood as the signature of the azimuthal (poloidal) field component in an emerging flux rope. They are present as long as the top horizontal portion of the twisted flux tube (called apex from now on) is crossing the photosphere. The spatial organization of the magnetic tongues and the orientation of the polarity inversion line (PIL) can be used as proxies of the magnetic helicity sign of the emerging field.

Magnetic tongues are observed in the early phase of emergence of an AR. Many clear observed examples of tongues have been published in previous papers, either recognized or overlooked by their authors. In the explicit cases, the helicity sign inferred from the tongues in the studied ARs was found to be in agreement with all the other proxies of the magnetic helicity sign listed hereafter (for reviews, see *e.g.* Pevtsov, 2002, and Démoulin and Pariat, 2009). First, the most direct proxy for the determination of the helicity sign is the magnetic shear along the PIL as measured from photospheric vector magnetograms (*e.g.*, Li *et al.*, 2007; Canou *et al.*, 2009). Second, a directly related proxy is the observed shear (inclination with respect to a perpendicular direction over the PIL) of an arch filament system (an indication of emerging field, *e.g.* Strous *et al.*, 1996; Asai

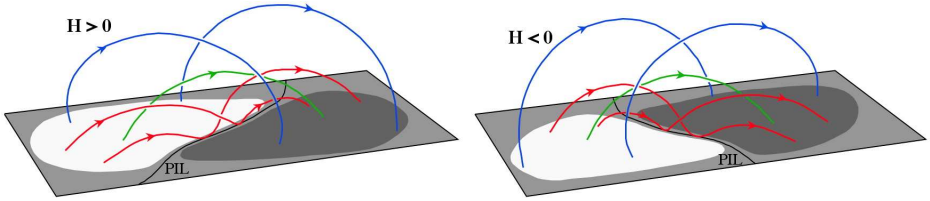

Figure 1. Sketch of the magnetogram of the vertical (perpendicular to the photospheric plane) field component during the emergence of a twisted flux tube. As the apex of the flux tube emerges, two elongated magnetic polarities, called magnetic tongues, develop. The spatial organization of the tongues resembling the *yin yang* pattern indicates the sign of the magnetic helicity, independently of the sign of the magnetic polarities (positive/negative for white/dark grey, respectively). Some enveloping arcade and internal dipped field lines are shown with blue/green and red lines, respectively.

et al., 2009). A third proxy is the shear observed in coronal loops (*e.g.*, Burnette, Canfield, and Pevtsov, 2004; Tian *et al.*, 2005b; Cristiani *et al.*, 2008). Fourth, there is frequently a spatial shift of the ribbons of an eruptive (or so-called two-ribbon) flare along the PIL (this is an indication of the remaining magnetic shear present after reconnection as the ribbons are linked by flare loops) and, in some cases, the ribbons have a J-shape (an indication of reconnection at the periphery of a flux rope, *e.g.* Démoulin, Priest, and Lonie, 1996; Chandra *et al.*, 2009). Finally, the photospheric magnetic helicity flux injected in an AR can be computed from longitudinal magnetograms using the local correlation tracking technique (*e.g.*, Chae, Moon, and Park, 2004; Yamamoto *et al.*, 2005; Jeong and Chae, 2007; Liu and Zhang, 2006; Yang, Büchner, and Zhang, 2009a). All these proxies of the magnetic helicity sign have been used in a much broader set of publications; however, only the few examples cited above show explicitly the magnetic tongues.

The presence of magnetic tongues has also been associated with coronal sigmoids in a few cases (Mandrini *et al.*, 2005; Tian and Alexander, 2006; Green *et al.*, 2007). Sigmoids are best observed in soft X-rays (Rust and Kumar, 1996; Canfield, Hudson, and McKenzie, 1999; Glover *et al.*, 2000; Pevtsov, 2002). They are the coronal tracers of twisted or, at least, highly sheared field lines. Indeed, when the photospheric magnetic helicity has a well marked dominant positive (negative) sign, a forward (backward) sigmoid is typically observed, respectively (Pevtsov, Canfield, and McClymont, 1997; Burnette, Canfield, and Pevtsov, 2004). Sigmoids are presently understood as tracers of the border of twisted flux ropes formed by reconnection of highly sheared magnetic arcades (Green *et al.*, 2007; Green and Kliem, 2009; Archontis *et al.*, 2009; Aulanier *et al.*, 2010).

The main objective of the present paper is to further analyze the presence and evolution of magnetic tongues during the emergence of 40 ARs and to relate them to sigmoids and/or sheared coronal loops. Other proxies of the magnetic helicity sign are also used whenever available. We first describe the selection criteria of ARs for analysis and the observations used (Section 2). Then, we analyze the evolution of magnetic tongues in a set of six emerging bipoles (Section 3). The physical interpretation of magnetic tongues, as well as the limitations in

their use are discussed in Section 4, with details of a simple analytical model of the magnetic tongues presented in the Appendices A and B. We show some quantitative analysis of the tongues in Section 5. Finally, we summarise and conclude, making links between twisted flux emergence and coronal mass ejections (CMEs), emphasising the importance of the simple recognition of helicity sign for, *e.g.*, space weather purposes (Section 6).

2. Observations and Data Analysis

2.1. Data Selection

Though tongues should develop during the emergence of a significantly twisted flux tube, their presence and temporal evolution are not always clearly observable. In principle, tongues are present during the first stages of flux emergence; therefore, the examples included in this study correspond to bipoles that appeared on the solar disk on the eastern hemisphere (in general at a few tens of degrees from the east limb). These bipoles should emerge isolated, far from any other significantly intense flux concentration or, at least, their flux should increase fast enough to be visible within a pre-existing flux concentration (such as an AR). This condition excludes from our data set cases in which bipoles emerge in complicated nests of ARs.

The examples in this study are those for which we could find sufficiently broad magnetic data coverage and, at least, one other proxy to confirm the magnetic helicity sign derived from the shape of tongues. To achieve this, we extensively reviewed the literature and collected ARs which fulfilled our selection criteria and for which the helicity sign was determined.

2.2. Instrument Description

We follow the evolution of the photospheric magnetic field using data from the Michelson Doppler Imager (MDI, Scherrer *et al.*, 1995) on board the *Solar and Heliospheric Observatory* (SOHO). MDI measures the line-of-sight (or longitudinal) magnetic field in the mid-photosphere. We use full-disk magnetograms with a 96-minute cadence. The measured magnetic field is the field averaged over a magnetogram pixel with a size of 1.98 arcsec. All the data are differentially rotated to the time of central meridian passage.

The EUV emission of coronal loops is analyzed using data from the SOHO/-Extreme Ultraviolet Imaging Telescope (EIT, Delaboudiniére *et al.*, 1995). EIT observes the full Sun regularly with four different filters and with a pixel size of 2.6 arcsec. We use mainly the 195 Å band ($T \approx 1.5 \times 10^6$ K) since it has typically the highest time cadence (down to 12 min) and because coronal loops are well seen in this wavelength range.

The Soft X-ray Telescope (SXT), on board *Yohkoh*, (Tsuneta *et al.*, 1991) is used to identify the hottest coronal loops (above 2×10^6 K). SXT was a grazing incidence telescope that formed X-ray images in the 0.25 to 4.0 keV energy range, which corresponds to a wavelength range of 3–60 Å. Full-disk SXT data, taken with the Dagwood (AlMg), are used in this work.

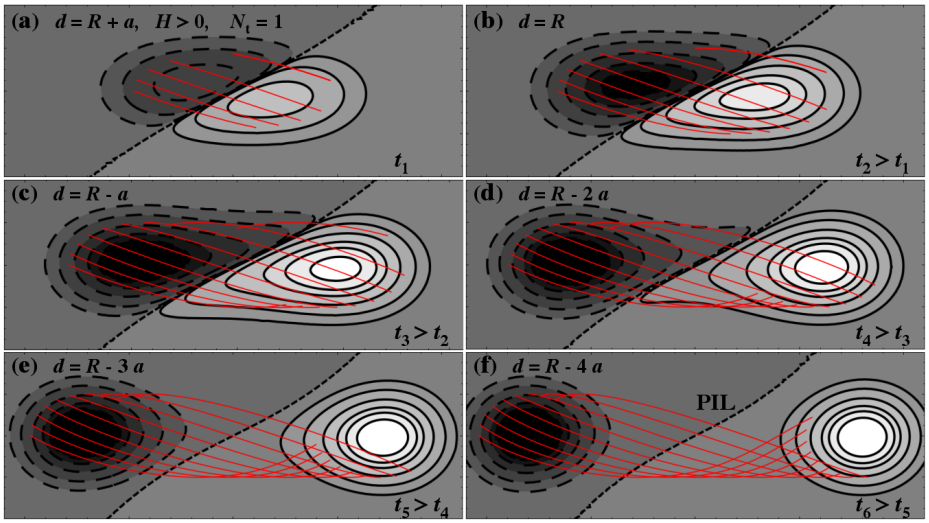

Figure 2. Temporal evolution of the magnetic tongues during the emergence of a twisted flux tube computed from a simple model having a torus shape, see Appendix A. The magnetic helicity is positive (the case with negative helicity mirrors this one). Some field lines are drawn in red to outline the magnetic configuration. Notice that, with an uniform twist, the direction of the central part of the PIL does not change while the bipole shows an apparent rotation due to the retraction of the tongues.

3. Emergence of Active Regions

3.1. Magnetic Tongues

Magnetic tongues are defined as elongations of the magnetic polarities which can be observed during the emergence of, at least, a fraction of ARs (López Fuentes *et al.*, 2000). There are only two basic configurations of magnetic tongues as shown in Figure 1. They are associated with positive or negative magnetic helicity signs, when the flux distribution is interpreted as due to the emergence of a twisted flux tube (see Section 4.1). If the sign of the magnetic polarities is reversed in Figure 1, the sign of the magnetic helicity does not change, i.e. the tongues represent a polarity-invariant helicity-proxy. A typical evolution of the magnetic tongues, as the flux rope is emerging, is shown in Figure 2 for a simple model defined in Appendix A. In the following sections we present several examples of such magnetic tongues in ARs emerging in zones with no significant pre-existing magnetic flux. We begin with a simple case before analyzing more complex ones.

3.2. Evolution of AR 8203

AR 8203 emerges in the quiet Sun (see the movie 8203_mdi.mpg in the electronic supplement). The tongues are not visible at the beginning of the emergence and the bipole is almost east-west oriented (first panel of Figure 3). Long magnetic tongues develop later on (from late 14 April to 16 April). The tongues have

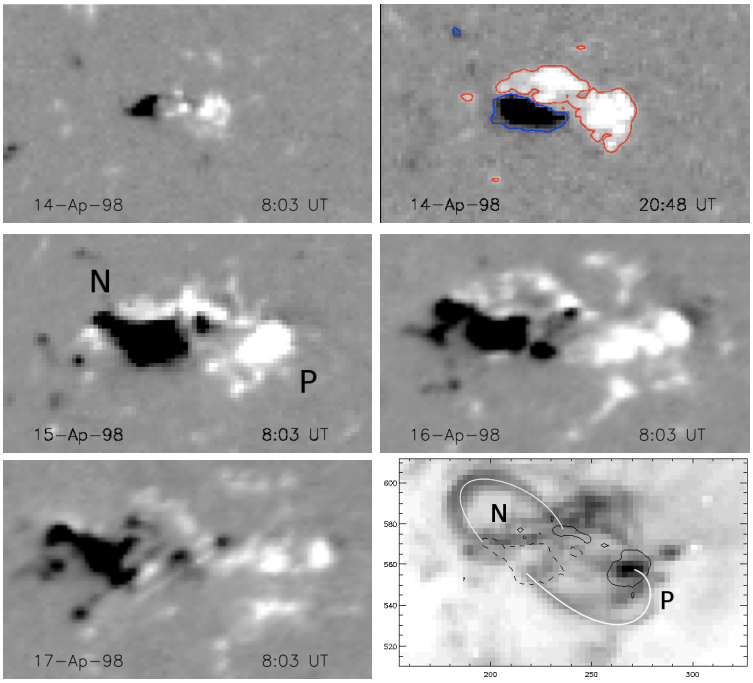

Figure 3. Photospheric magnetograms from SOHO/MDI showing the evolution of the magnetic tongues in AR 8203, together with a contrast-enhanced reversed image taken with EIT in 195 Å (at 07:14 UT on 15 April 1998) with two isocontours of the magnetic field (±300 gauss (G)) superposed. Two coronal loops are highlighted with hand-drawn white lines. The magnetograms have been rotated to the central meridian position of the AR (positive/negative magnetic field polarities are indicated in white/black colour). The magnetic tongues indicate negative magnetic helicity; they are outlined with ±100 G isocontours on the top right panel. The main polarities are labeled in the magnetogram closest in time to the 195 Å image. The field of view is the same in all panels.

almost disappeared by 17 April, when the photospheric magnetic flux starts to decrease (Figure 7d). The tongues indicate a negative magnetic helicity (*c.f.* Figure 1) in agreement with the sign deduced from the sheared loops observed with EIT in 195 Å (Figure 3).

3.3. Evolution of AR 8011

AR 8011 emerges as a small bipole and has magnetic tongues indicating positive magnetic helicity (see the movie, 8011_mdi.mpg, from 3:15 to 6:27 UT on 13 January in the electronic supplement). Later, on the same day, no significant tongues are present (*e.g.* Figure 4 at 20:48 UT on 13 January). However, tongues become again identifiable on the next day as new magnetic flux emerges. Their presence is not clear at the beginning (*e.g.* at 8:03 UT on 14 January), while they are well seen later on (*e.g.* at 20:51 UT on 14 January). Both the spatial organization of the tongues and the associated soft X-ray sigmoid indicate positive magnetic helicity. As the AR evolves, the magnetic polarities separate and the magnetic

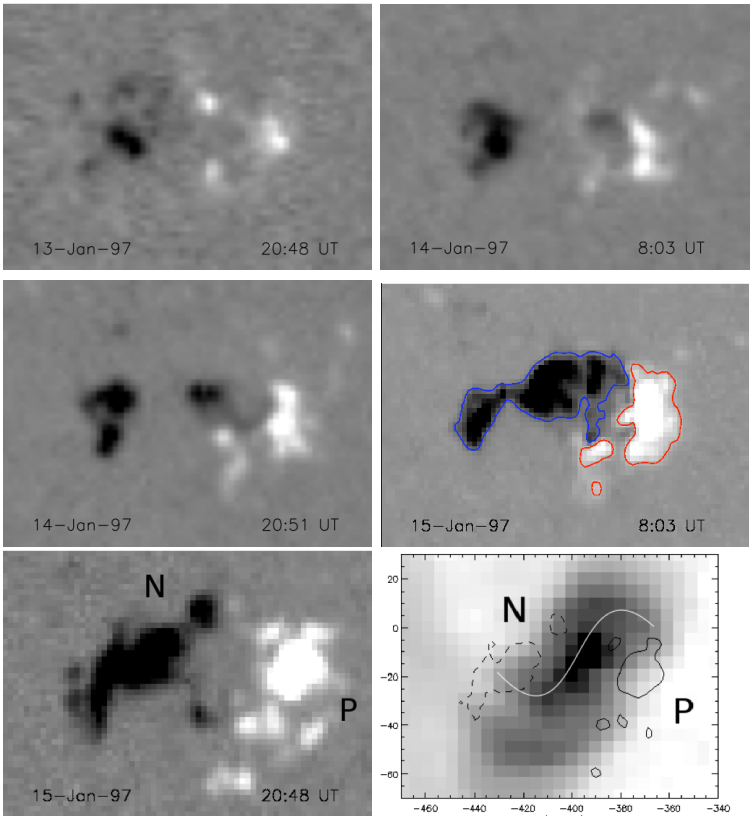

) with two isocontours of the magnetic field superposed (±300 G). The X-ray sigmoid is highlighted by a hand-drawn S-shaped white line.

Figure 4. Same display as in Figure 3 for AR 8011. The magnetic tongues indicate positive magnetic helicity (outlined with ± 100 G isocontours in the middle right panel). The lower right panel is a contrast-enhanced reversed image taken in soft X-rays (*Yohkoh*/SXT image at 22:20 UT on 15 January 1997

tongues retract again. The tongues disappear when the magnetic flux of both polarities reaches maximum in the morning of 16 January (Figure 7a).

The injection of magnetic helicity, computed from the time evolution of MDI magnetograms, shows an overall positive injection during almost the entire day on 14 January (Figure 2, panel A2 of Yamamoto *et al.*, 2005), when the magnetic tongues are well visible. Later, at the beginning of 15 January, the injection of helicity becomes negative but with much smaller flux values. The maximum injected helicity is about 14×10^{40} Mx^2 (Mx: maxwell), taking into account the magnetic flux measurements of Figure 7a (in which the re-calibration of MDI data is included). Later on, around 17 January, Chae (2001) found a globally positive, but weaker injection, of about 2.4×10^{40} Mx^2 during 39h.

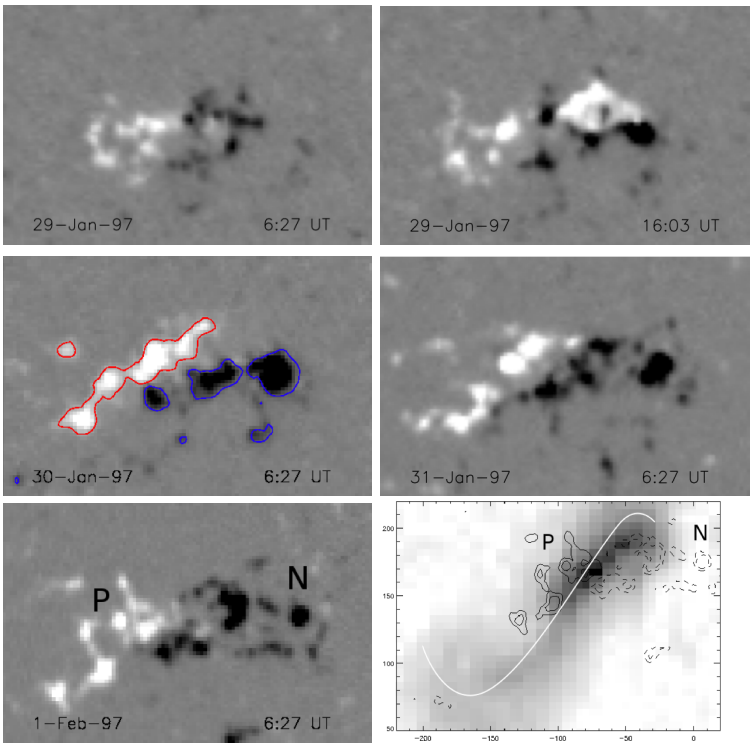

Figure 5. Same display as Figure 3 for the second bipolar emergence in AR 8015 (called 8015b). The magnetic tongues indicate positive magnetic helicity (± 100 G isocontours in the middle left panel). The X-ray sigmoid, observed with *Yohkoh*/SXT (on 1 February 1997 at 06:06 UT), is highlighted by a hand-drawn S-shaped line in the lowest right panel. The sigmoid extends well outside the AR main magnetic field concentrations.

3.4. Evolution of AR 8015

By the beginning of the movie 8015_mdi.mpg, AR 8015 consists of an evolved bipole that we call 8015a. This bipole still shows magnetic tongues, indicating a positive helicity sign (*e.g.* Figure 5 at 6:27 UT on 29 January). The emergence of a new bipole, called 8015b, starts around 8:00 UT on 29 January within the previous bipole. This second bipole has well-developed magnetic tongues from the beginning of its emergence up to ≈ 8:03 UT on 1 February (Figure 5). The spatial organization of the flux in the tongues indicates again positive helicity, in agreement with the sign deduced from the observed soft X-ray sigmoid. The tongues reach a maximum extension along the PIL by the end of 30 January when the magnetic flux of both polarities reaches its maximum (Figure 7b).

A third bipole emerges at the same location at the beginning of 2 February (Figure 6). Its magnetic flux cancels the previous bipole flux, rapidly becoming dominant, so that we can study this third bipole as if it were emerging in the quiet Sun (Figure 7b). The new bipole develops long magnetic tongues that progressively disappear by the beginning of 4 February, when the magnetic flux is at maximum. The magnetic tongues of this third emergence episode indicate an

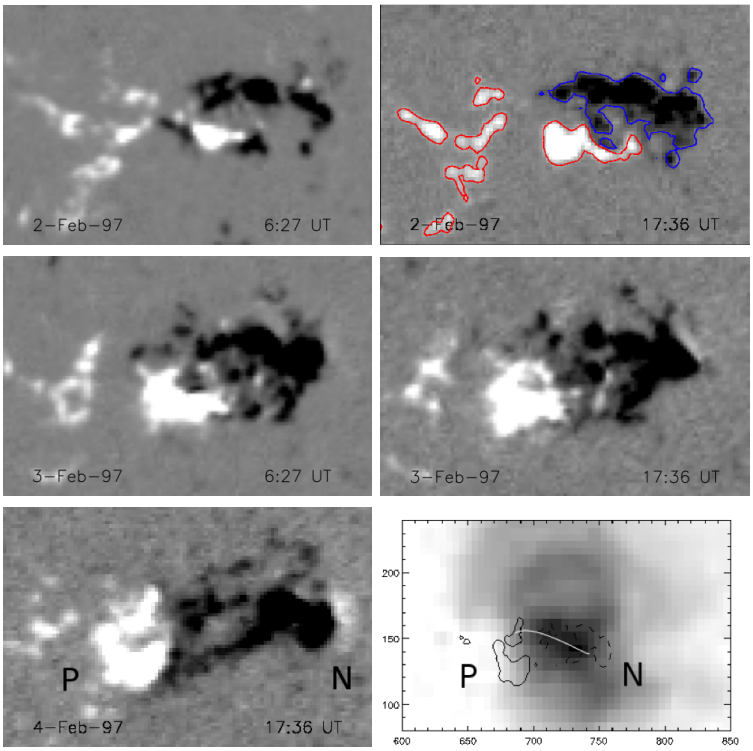

Figure 6. Same display as Figure 3 for the third bipolar emergence in AR 8015 (called 8015c). The magnetic tongues indicate negative magnetic helicity (± 100 G isocontours in the top right panel). The sheared arcade of X-ray loops, observed with *Yohkoh*/SXT (at 17:26 UT on 4 February 1997), is highlighted by one hand-drawn line in the lowest right panel showing that the magnetic helicity sign in the corona is negative.

opposite magnetic helicity sign to that of the first two bipoles. This is, indeed, confirmed by the negative magnetic shear displayed by the soft X-ray loops (Figure 6).

Our inference of the magnetic helicity sign is in good agreement with the injection of magnetic helicity computed for the second and third bipoles in AR 8015 (see Figure 2, panel B2 in Yamamoto *et al.*, 2005). We conclude that this AR showed a peculiar behaviour represented by the successive emergence of at least three bipoles with a common toroidal (east-west) field; the first two bipoles carried positive magnetic helicity, while the last one carried helicity with opposite sign. While it appears peculiar, this evolution can be quite common in the so-called activity nests. For example, the AR studied by Chandra *et al.* (2010) was formed by several magnetic bipoles with mixed helicity signs. Simply, in AR 8015, we have the opportunity to observe the bipoles emerging well-separated in time so that each of them can be clearly identified.

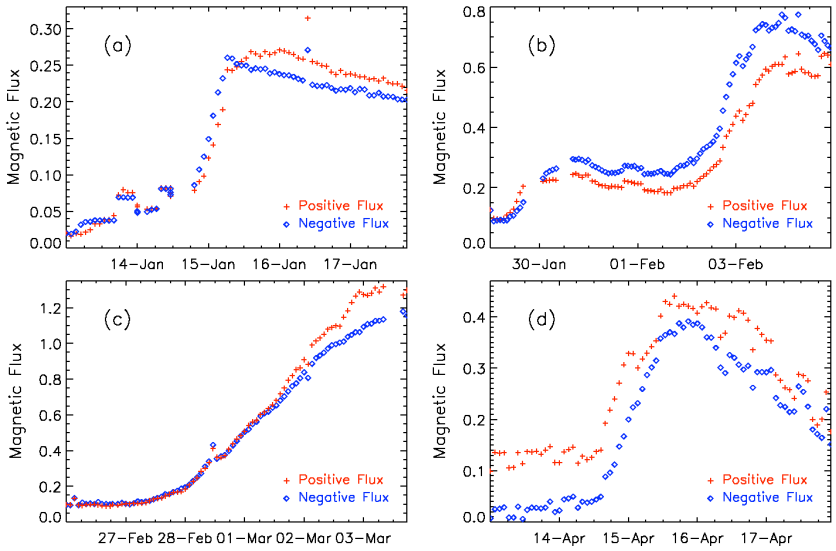

Figure 7. Magnetic flux evolution during the emergence of (a) AR 8011 (Figure 4), (b) AR 8015 (both bipoles, Figures 5,6), (c) AR 8171 (Figure 8), and (d) AR 8203 (Figure 3). Magnetic flux is in units of 10^{21} Mx.

3.5. Evolution of AR 8171

AR 8171 emerges in the quiet Sun. The tongues are well marked from the beginning of the emergence and the bipole is oriented nearly in the north-south direction (central part in the first panel of Figure 8). These tongues extend later (on 27 February, Figure 8); then, they shrink (on 28 February) and, finally, they almost disappear on 1 March leaving an almost east-west bipole (see the movie 8171_mdi.mpg in the electronic supplement).

Later, on 2 March, magnetic tongues grow again to become very prominent on 3 March (movie 8171_mdi.mpg). During all this evolution, new magnetic flux is continuously emerging (Figure 7c). The tongues indicate positive magnetic helicity in both time intervals, in agreement with the sheared loops observed with EIT in 195 Å (the coronal loops are sheared compared to a potential field extrapolation). Leamon, Canfield, and Pevtsov (2002) associated a magnetic cloud formed by a left-handed (*i.e.* negative helicity) flux rope to this AR, *i.e.* having the opposite sign of magnetic helicity indicated by the tongues. We find no evidence of negative helicity neither at the photospheric nor at the coronal levels. However, this case might be similar to the one analyzed by Chandra *et al.* (2010), *i.e.* an AR with mixed magnetic helicity, or the magnetic cloud may have a different solar source.

3.6. Evolution of AR 8757

AR 8757 has a similar evolution to that of AR 8203, except that the initial bipole is tilted (inclined compared to the east-west direction) and the helicity sign is the opposite (movie 8757_mdi.mpg in the electronic supplement and Figure 9).

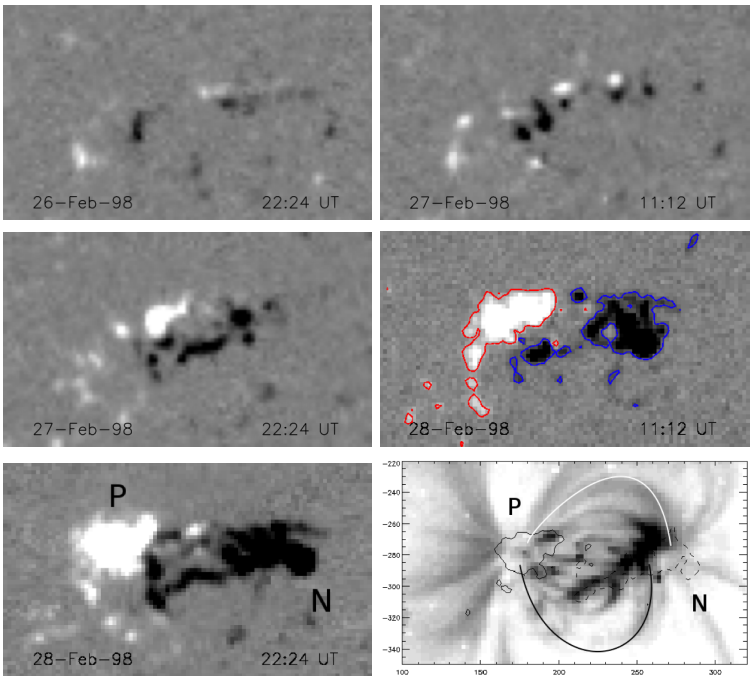

Figure 8. Same display as in Figure 3 for AR 8171. The magnetic tongues indicate positive magnetic helicity (± 100 G isocontours in the middle right panel). The sheared EUV loops, observed with SOHO/EIT in 195 Å (at 07:31 UT on 1 March 1998) are shown in the lower right panel with hand-drawn white and black lines. They indicate that the magnetic helicity sign in the corona is positive.

Moreover, since there are multiple episodes of flux emergence, the magnetic tongues have a cyclic behavior with a repetition of the sequence of elongation and shrinkage, as follows. Tongues are present on 5 November at 06:00 UT, they grow and then retract to become undetectable about 17 hours after. On the next day a similar episode starts at about 12:00 UT to end about one day later. Finally, new tongues are observed at the beginning of 10 November but we cannot see their retraction, since the AR was by then too close to the west limb. The magnetic tongues indicate positive magnetic helicity, in agreement with the sign deduced from the sheared coronal loops observed with SXT (Figure 9).

3.7. Evolution of Other ARs

The results for all the 40 ARs studied are summarised in Table 1. As for the example ARs shown in the figures, we have analyzed the magnetic field evolution during their emergence. We have checked if a sigmoid, or at least sheared coronal loops, were present in EUV or soft X-rays. We have also searched for other proxies of the magnetic helicity sign such as photospheric vector magnetograms, sheared arch filament systems, sheared coronal loops, as well as *in situ* magnetic field measurements in a magnetic cloud related to the studied ARs (see Figure 1 of Démoulin and Pariat, 2009; Luoni *et al.*, 2007). We have also used the previously published results of photospheric magnetic helicity flux injection, which

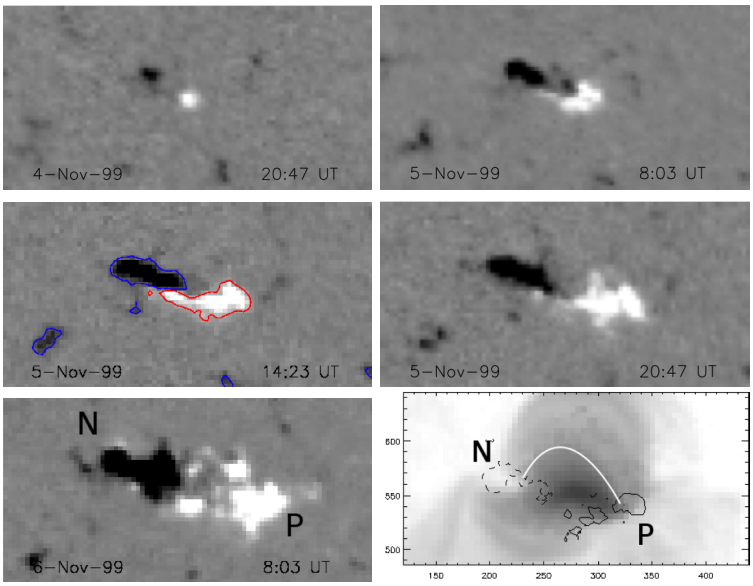

Figure 9. Same display as in Figure 3 for AR 8757. The magnetic tongues indicate positive magnetic helicity (± 100 G isocontours in the middle left panel). The sheared coronal loops, outlined with a hand-drawn white line, are shown in the lowest right panel with a contrast-reversed image obtained with *Yohkoh*/SXT (at 05:15 UT on 8 November 1999).

is computed from the evolution of longitudinal magnetograms using the local correlation-tracking technique. We have found that the helicity sign given by the magnetic tongues agrees, in all but one case out of 40, with the helicity sign inferred from these other proxies.

It is worth mentioning that the last AR included in the table (AR 11060) is the one in which a CME, observed with unprecedented temporal and spatial resolution by the Atmospheric Imaging Assembly (AIA) on board the *Solar Dynamic Observatory*, occurred on 8 April 2010. Magnetic tongues are clearly seen from 5 April 2010 in MDI magnetograms (see http://soi.stanford.edu/production/mag_gifs.html), their shape indicates positive magnetic helicity. The tongues progressively retract and disappear by late 9 April. The EUV post-flare loops, as well as the shape of the flare ribbons (see http://sdo.gsfc.nasa.gov/assets/img/firstlight/movies/multiwave_zm_sm.mov), indicate that the coronal magnetic helicity is also positive. Two ARs included in Table 1 present a particular behaviour that we discuss in the next paragraphs.

AR 9563 is the only case in Table 1 for which the helicity sign deduced from the tongues and other proxies did not match. The distribution of the magnetic flux in the tongues indicates that, before its central meridian passage on 5 August 2001, its magnetic helicity is negative; the same helicity sign can be inferred from the X-ray loops observed with SXT. However, Tian and Alexander (2009) reported that a positive helicity injection occurred mostly after 6 August. In fact, a second bipole emerged in the center of this AR on that day; this bipole had positive magnetic helicity opposite to that of the first bipole (see the corresponding panel in Figure 6 of Tian and Alexander (2009), and MDI magnetograms in

the previously mentioned web page). This evolution is similar to the one of AR 8015 (Section 3.4); the main differences are that the first bipole does not disperse sufficiently by the time of the second flux emergence and that the second bipole has a weaker magnetic flux (a factor ≈ 0.2) compared to the first one. So, conversely to AR 8015, the second bipole emergence with the opposite helicity sign in AR 9563 is mixed up with the first bipole; therefore, its magnetic tongues cannot be clearly identified.

AR 10030 appears on the solar disk on 10 July 2002 as an already evolved and extended region formed by two bipoles. The tongues to which we refer in Table 1 correspond to the emergence of a third bipole towards the east of the main positive sunspot, as discussed in Tian and Alexander (2008); these are clearly observed in Figure 10 of that paper. The loops observed with EIT in 195 Å confirm that the coronal magnetic helicity is negative, as is the helicity of the bipoles present before this emergence (see Tian and Alexander, 2008).

4. Interpretation

4.1. Emergence of a Twisted Flux Tube

MDI magnetograms provide the evolution of the longitudinal component of the photospheric magnetic field. Since we restrict the study to ARs close to disk centre, the main contribution to the magnetic signal comes from the vertical (perpendicular to the photospheric plane) component of the magnetic field. There is no information on the magnetic shear (which requires vector magnetograms). However, when the emerging flux tube is twisted an asymmetry appears in the photospheric spatial distribution of the vertical magnetic field due to the contribution of the azimuthal component. The result is schematically depicted in Figure 1 and the photospheric evolution of the tongues is shown in Figure 2 for the emergence of a flux tube carrying positive magnetic helicity.

The projection of the flux rope azimuthal (poloidal) field component on the vertical direction results in two elongated polarities, called magnetic tongues, which extend between the strongest opposite polarity concentrations forming an *yin yang* pattern. Their relative position depends on the sign of the twist (Figure 1). For a given geometry of the emerging flux tube, the extension of these tongues increases with the magnitude of the twist, as we show in the Appendix B. The tongues are present only while the apex of the flux tube is crossing the photosphere, *i.e.* during the period of flux emergence (when the magnetic flux of both polarities is increasing). Later on, the tongues disappear because the projection of the azimuthal field on the vertical direction becomes less important. Finally, the retraction of the tongues with time in emerging ARs, shown in Section 3, is naturally explained by this model (see Figure 2). They retract and disappear when the apex of the flux tube has fully crossed the photosphere, *i.e.* when the maximum flux is reached in both photospheric polarities. After that, decay sets in and the magnetic flux of the simple bipolar AR progressively disperses with time.

The simplest model, representing the evolution just described, is analytical and considers a magnetic field confined in a torus (see the Appendix A). The

Table 1. Summary of results for the entire sample of 40 ARs. The magnetic helicity sign inferred from the magnetic tongues is given in the third column. In the fourth column, S and Z letters are for forward and backward sigmoids (an indication of positive and negative helicity, respectively), while the + and − symbols represent the helicity sign deduced when only sheared coronal loops are present. The sign of $H_{\rm Bt}$ is inferred from vector magnetograms, that of $H_{\rm inj}$ from the evolution of longitudinal magnetograms (computation of helicity injection), the one of $H_{\rm rib}$ from the spatial shift of flare ribbons along the PIL, that of $H_{\rm MC}$ from the helicity of the associated magnetic cloud, and the one of $H_{\rm mod}$ to the sign of α in a linear force-free ($\nabla \times \mathbf{B} = \alpha \mathbf{B}$) model of the AR.

AR	First appearance	Magnetic helicity Sign			Ref.[a]
		Tongues	Sigmoid or loops	Other proxies	
8011	13/01/97	+	S	$H_{\rm inj} > 0$	3,21
8015	29/01/97	+	S	$H_{\rm inj} > 0$	21
8015	02/02/97	−	Z	$H_{\rm inj} < 0$	21
8016	01/02/97	+	+	$H_{\rm inj} > 0$	12,22
8027	03/04/97	+	S	$H_{\rm MC} > 0$	1,2,9,12
8032	14/04/97	+	S	$H_{\rm MC} > 0$	7,12
8038	06/05/97	−	Z	$H_{\rm inj}, H_{\rm MC}, H_{\rm rib} < 0$	9,12,21
8059	01/07/97	+	+	$H_{\rm inj} \approx 0, H_{\rm MC} > 0$	12,21
8064	23/07/97	−	−		
8066	25/07/97	−	Z	$H_{\rm MC} < 0$	12
8086	12/09/97	+	S		
8100	27/10/97	−	−	$H_{\rm Bt} < 0$	8,14,17
8171	26/02/98	+	+	$H_{\rm MC} < 0$	12
8176	07/03/98	−	−		
8203	13/04/98	−	Z		20
8214	29/04/98	+	+	$H_{\rm inj} > 0$	17,19
8232	03/06/98	+	S		
8375	30/10/98	+	S	$H_{\rm inj}, H_{\rm MC} > 0$	15,17,19
8611	27/06/99	−	−	$H_{\rm inj} < 0$	19
8757	05/11/99	+	S		
8760	07/11/99	−	−	$H_{\rm inj} > 0$	17,19
8771	18/11/99	−	−	$H_{\rm inj} < 0$	17
8910	13/03/00	+	+	$H_{\rm inj} > 0$	17,19
9114	05/08/00	−	Z	$H_{\rm inj}, H_{\rm MC} < 0$	6,15
9139	19/08/00	−	−	$H_{\rm inj} < 0$	19
9563	01/08/01	−	−	$H_{\rm inj} > 0$	17,19
9574	09/08/01	+	+	$H_{\rm inj} > 0$	19
9684	29/10/01	−	Z	$H_{\rm inj} < 0$	16,17
9715	24/11/01	+	+	$H_{mod} > 0$	23
9906	10/04/02	+	+	$H_{\rm inj} > 0$	19
10030	10/07/02	−	−	$H_{\rm Bt}, H_{\rm rib} < 0$	18
10050	26/07/02	+	+	$H_{\rm inj} > 0$	17
10226	13/12/02	+	+	$H_{mod} > 0$	24
10365	20/05/03	+	+	$H_{\rm inj}, H_{\rm rib} > 0$	4,5,10,11,17
10381	09/06/03	−	−	$H_{\rm inj} < 0$	10
10488	26/10/03	−	−	$H_{\rm inj}, H_{\rm rib} < 0$	13,17
10656	06/08/04	−	−	$H_{\rm inj} < 0$	10,19
10696	02/11/04	−	−	$H_{\rm inj} < 0$	10
10720	11/01/05	+	+	$H_{\rm Bt} > 0$	14
11060	04/04/10	+	+		

[a] The results in the fifth column are from: 1: Attrill *et al.* (2007), 2: Berdichevsky *et al.* (2002), 3: Chae (2001), 4: Chae, Moon, and Park (2004), 5: Chandra *et al.* (2009), 6: Georgoulis and LaBonte (2006), 7: Gopalswamy *et al.* (2000), 8: Green *et al.* (2002), 9: Green *et al.* (2007), 10: Jeong and Chae (2007), 11: LaBonte, Georgoulis, and Rust (2007), 12: Leamon, Canfield, and Pevtsov (2002), 13: Liu and Zhang (2006), 14: Liu, Zhang, and Zhang (2008), 15: Nindos, Zhang, and Zhang (2003), 16: Tian and Alexander (2006), 17: Tian and Alexander (2008), 18: Tian, Alexander, and Nightingale (2008), 19: Tian and Alexander (2009), 20: Wu *et al.* (2005), 21: Yamamoto *et al.* (2005), 22: Yang, Zhang, and Büchner (2009b), 23: Cristiani *et al.* (2007), 24: Cristiani *et al.* (2008).

field is uniformly twisted, both across and along the flux tube. In this model, the PIL between the opposite polarities is a straight segment which is less inclined with respect to the line connecting the main photospheric polarities when the twist increases (Figure 13). Also as the twist increases, the magnetic tongues become more elongated. They are prominent for a twist larger than one turn.

The simple model, discussed above, and described in detail in Appendix A, does not consider either the force balance or the strong fragmentation of the twisted flux tube as it tries to cross the photosphere. However, since the magnetic tongues are associated with the global structure of the flux rope (its global twist), magnetic tongues are still present even if the flux rope becomes strongly fragmented as it crosses the photosphere, and even if it emerges in narrow threads and at multiple locations (appearing as small-scale flux emergence), reconnection can restore it in its original length, as shown by all the MHD simulations described in the next paragraphs. Such simulations, so far, consider only one coherent flux tube in the CZ, while Parker (1979) argued that the magnetic field is split into a bundle of many smaller flux tubes below sunspots. Magnetic tongues are also expected if such bundle of flux tubes is present in the CZ as long as the bundle is globally twisted. Then, magnetic tongues would reflect such global twist (and not the individual twist of each flux tube). Such global twist would be needed to keep a coherence as the bundle of flux tubes crosses the CZ.

The initial configuration used by the majority of the numerical simulations is a very twisted horizontal flux tube located below the photosphere. It is typically set more buoyant in the central part, so it rises faster there. Both because of the high twist and the weak bending of the flux tube, prominent magnetic tongues are typically found in such simulations, as in the case of the simple model with large twist (*e.g.*, Figure 8 in Magara and Longcope, 2003; Figure 9 in Archontis *et al.*, 2004; Figure 2 in Manchester *et al.*, 2004; Figure 8 in Fan, 2009; Figure 14 in Murray and Hood, 2008). As the top part of the flux rope emerges above the photosphere, the tongues become very elongated and thin. Such extreme case of very extended tongues is not frequently observed (see the examples given in Figures 4-6, 8-9), but it is indeed present in some large and strong-field ARs though they are less conspicuous than in most MHD simulations (Chae, Moon, and Park, 2004; Li *et al.*, 2007; Canou *et al.*, 2009). The MHD simulations of Archontis and Hood (2010) sucessfuly reproduce the main characteristics of the evolution of such large tongues dubbed as magnetic tails observed in the AR studied by Canou *et al.* (2009).

At present, the MHD simulations that better reproduce the observed magnetic tongues start with a bent (arched) flux tube (half a torus), or a straight flux tube with a sufficiently enhanced magnetic buoyancy, such that the axis of the flux tube is significantly arched upward when it reaches the photosphere. Such setup also lets the full flux rope cross the photosphere more easily, as the dense plasma is no longer caught in magnetic dips, and it also implies a finite maximum separation of the polarities as observed (Hood *et al.*, 2009; MacTaggart and Hood, 2009). The simulated magnetograms shown in Figures 2 and 4 of Hood *et al.* (2009) have an evolution of the magnetic tongues similar to the ones found in emerging ARs, such as those shown in Figures 4-6, 8-9 (however, the magnetic

flux in these ARs is typically 2 to 10 times larger than in the above numerical simulations).

4.2. Magnetic Helicity

The largest photospheric injection rate of magnetic helicity in ARs is typically found associated with the largest increase of magnetic flux. When the emergence of the AR is monitored from its beginning, a peak in the helicity rate is usually found such as in Figure 5 of Chae, Moon, and Park (2004), Figure 2 of Yamamoto *et al.* (2005), Figures 1–3 and 6 of Jeong and Chae (2007), and Figures 1–4 of Tian and Alexander (2008).

A comparable peak in the helicity rate is also found in the simple model of a toroidal field emerging at a constant velocity, see Figure 9 of Pariat, Démoulin, and Berger (2005). The peak of the helicity injection rate is obtained when the bottom of the apex of the flux tube crosses the photosphere, *i.e.* just before the top of the flux tube has completely emerged. A qualitatively similar peak of helicity injection is found in MHD simulations of emerging twisted flux tubes (Cheung, Schüssler, and Moreno-Insertis, 2005; Cheung *et al.*, 2008). Then, the evolution of the magnetic tongues indicates the time interval when a large amount of magnetic helicity is injected in the corona. Later on, the injection of magnetic helicity is most probably continuing at a lower rate during most of the AR field dispersal (Démoulin *et al.*, 2002; Green *et al.*, 2002; Mandrini *et al.*, 2004); however, in this later phase Gibson *et al.* (2004) found that the local correlation-tracking technique yields an underestimation of the helicity injection by an order of magnitude (in a theoretical configuration simulating an AR).

4.3. Determination of the Helicity Sign

The presence of magnetic tongues during the emergence of an AR lets us determine the sign of the magnetic helicity of the flux rope forming the AR (Figures 1, 2). We define the acute angle, $\delta_{\rm IL}$, from the bipole axis toward the PIL in the central part of an AR. With the bipole axis oriented from the following to the leading polarity, the sign of $\delta_{\rm IL}$ is the helicity sign of the emerging twisted flux tube (see Appendix B). Since the evolution of the magnetic tongues implies an apparent rotation of the AR bipole, we define the bipole direction with the mean positions of the polarities (see Equation (7)) when the tongues are the least present, i.e. when the AR is the oldest. Typically, the PIL is complex in emerging ARs due to the serpentine nature of flux emergence. To determine the location of a mean PIL defined by significant magnetic field intensity values, we fit a linear function of the spatial coordinates to the central part of the AR magnetogram. Then, we equal the fitted function to zero which defines the PIL. We check that the defined straight line agrees with the mean direction of the field isocontours (*e.g.* $\pm$50 G (gauss)). The computed $\delta_{\rm IL}$ values confirm the sign of helicity deduced visually in Figure 3-6, 8 and 9. The evolution of $\delta_{\rm IL}$ is shown separately for positive and negative helicities in Figure 10.

During the emergence, magnetic helicity is progressively transported into the corona forming a sheared/twisted magnetic configuration. The observed coronal

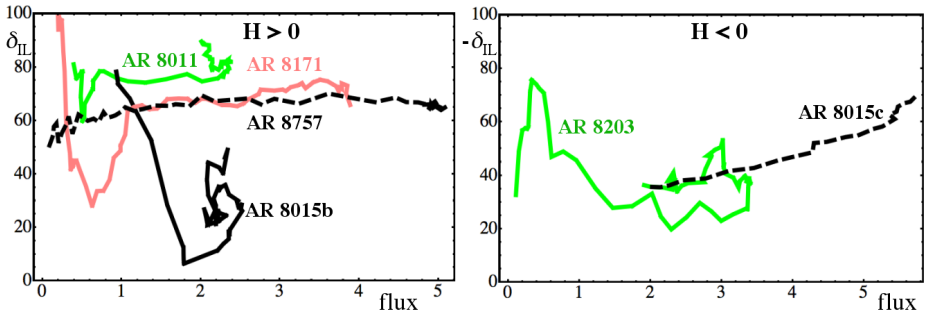

Figure 10. Evolution of the angle $\delta_{\rm IL}$ between the PIL and the bipole axis versus the mean magnetic flux of both polarities in units of 10^{21} Mx for the ARs shown in Figure 3-6, 8 and 9. The ARs are shown grouped according to their sign of magnetic helicity, H, as deduced from the sign of $\delta_{\rm IL}$. The last magnetogram of the time series studied is used to define the bipole axis. The magnetic flux of AR 8171 has been divided by a factor 3.

sheared loops and sigmoids are an evidence of this non-potentiality (*e.g.* Green *et al.*, 2007). We provide further examples in Table 1 where sigmoids have an S shape (resp. inverse S or Z shape) when the magnetic helicity sign, as inferred from the magnetic tongues, is positive (negative), respectively. This relationship is present if the sigmoids are formed by reconnection of a sheared arcade, building up a coronal twisted flux tube (Moore *et al.*, 2001; Titov and Démoulin, 1999; Green *et al.*, 2007; Aulanier *et al.*, 2010). We have also found that the helicity sign given by the magnetic tongues agrees with the helicity sign inferred from other proxies (Table 1).

When the axis of the emerging flux tube has a given geometry (curvature), the magnetic tongues are more extended and pronounced when the flux tube is more twisted. In the same way the extension of the tongues is smaller in the early phase of emergence if the emerging flux rope is less twisted at its periphery. Examples of such cases are given in Figures 4, 3, and 9, where the young bipole is almost aligned with the bipole present later on, after the disappearance of the magnetic tongues (so, in both cases the spatial distribution of the photospheric magnetic field is mainly due to the contribution of the axial field of the flux rope). However, we cannot quantify the amount of twist since the extension of the magnetic tongues also depends strongly on the curvature of the flux rope axis in a simple toroidal model and on the precise way the emergence proceeds in a more realistic model. Therefore, MHD simulations of flux emergence are needed to quantify the amount and the spatial distribution of the twist.

The magnetic tongues are only visible during the first stages of flux emergence, so they are best visible for ARs that start emerging on the eastern hemisphere (optimally at a few tens of degrees from the solar limb). This emergence has to be observed in a "clean" environment (that is to say, much more flux has to emerge than the already present background flux); furthermore, it has to be the single emergence of a globally twisted flux tube (which emerges in many pieces like a sea-serpent). For example, the magnetic tongues during the third emergence of AR 8015 (Figure 6) would not have been identified, or would have at least been difficult to interpret, if the second flux tube (Figure 5) would not have had

the time to significantly disperse and if the third bipole would have had a much weaker flux (see the magnetic flux evolution in Figure 7b). Such mixed helicity sign has been found in other ARs, for example AR 10501 (Chandra *et al.*, 2010); however, this particular AR is formed by a nest of bipoles so that magnetic tongues could not be unambiguously identified in the different emerging bipoles.

Finally, we notice that the interpretation of magnetic tongues can be ambiguous in some apparently simple bipolar ARs. For example, this is the case of AR 7978 (Démoulin *et al.*, 2002). While globally bipolar, the early stages of emergence in this AR are characterized by the appearance of several small bipoles giving a tongue-like pattern, characteristic of a negative magnetic helicity (see the panels from 8 to 10 July, 1996, in Figure 1 in Démoulin *et al.*, 2002). It is only by 11 July that the tongue pattern changes to indicate a positive helicity sign, in agreement with the magnetic shear of coronal loops (during this first solar rotation and the next ones). However, by that time the AR is close to the west limb, so that the magnetic field evolution cannot be observed and studied later on; furthermore, a significant amount of emergence occurs when the AR is behind the limb (as can be inferred from the magnetic flux present in the next Carrington rotation). This large AR starts emerging too close to the central meridian to allow us to identify clearly the complete evolution of the magnetic tongues. A closer examination of the magnetic evolution of AR 7978 shows the presence of a high-flux serpentine structure in the centre, involving the emergence of kinked-like U-loops, which significantly disturbs the tongue pattern. This implies that the tongue pattern in the early emergence phase of AR 7978 is not reliable. However, when emerging flux ropes are broken up into finer strands, the magnetic tongues remain more clearly recognisable.

5. Quantitative Analysis of the Magnetic Tongues

The orientation of the PIL, in the central part of an emerging bipole, with respect to the bipole axis is characterized by the angle $\delta_{\rm IL}$ (see Section 4.3. Considering the simple model of a uniformly twisted flux tube with a half torus shape, $\delta_{\rm IL}$ is directly linked to the number of field line turns, $N_{\rm t}$, present in the half torus (see Equation (6) in Appendix B). More generally, $\delta_{\rm IL}$ is related both to the twist per unit length and the local radius of curvature of the flux rope. For a given curvature radius, $|\delta_{\rm IL}|$ decreases from 90^0 (untwisted) toward 0^0 as the twist increases. The evolution of $|\delta_{\rm IL}|$ is shown in Figure 10 for six ARs. As for the simple model (Appendix A), $|\delta_{\rm IL}|$ stays mostly constant for three ARs (8011, 8171, 8757), apart from lower values in the early phase of emergence (a plausible indication of a larger twist at the border of the flux tube). ARs 8015b and AR 8203 rather show a progressive decrease of $|\delta_{\rm IL}|$, so a plausibly more twisted flux rope core, while AR 8015c has a reverse evolution with a slow increase of $|\delta_{\rm IL}|$ during the emerging phase. In all cases where the magnetic evolution could be followed long enough after the maximum flux was reached, $|\delta_{\rm IL}|$ evolved toward 90^0 as the magnetic tongues retracted. Converting these measured $\delta_{\rm IL}$ angles to the number of turns in a half torus with the model of the Appendix A, so using Equation (6), $|N_{\rm t}|$ values range from ≈ 0.1 (most of AR 8011 evolution), to

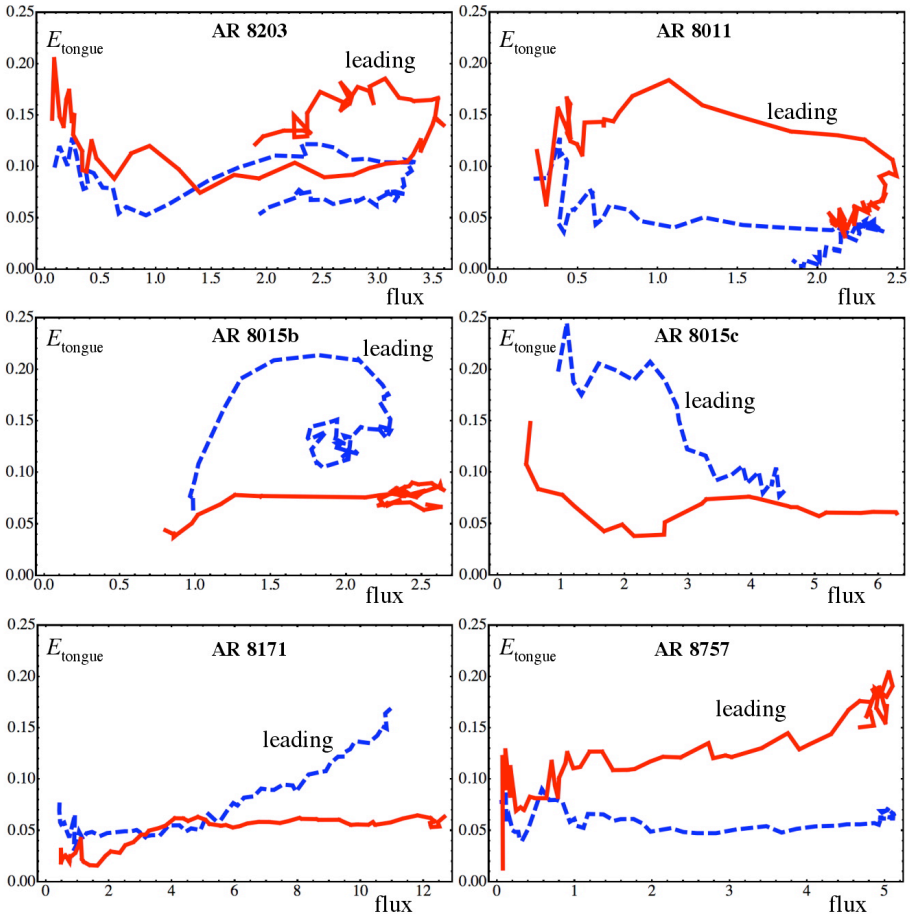

Figure 11. Evolution of the relative elongation of magnetic tongues, as defined by Equation (14), versus the magnetic flux in units of 10^{21} Mx for the ARs shown in Figure 3-6, 8 and 9. The color convention for the polarities is the same as in those figures. Notice that the leading magnetic polarity has typically a larger elongation than the following polarity.

≈ 0.2 (most of AR 8171 and 8757 evolutions), up to ≈ 3 for AR 8015c (maximum value). This indicates a broad range of twist (or a very significant effect of the flux rope geometry).

In the Appendix B we show that the elongation of the magnetic tongues is a function of the global twist. In an attempt to quantitatively analyse the observed tongues, we measure their relative elongations, as defined in Equation (14), in the six ARs as they emerge and plot the results as a function of magnetic flux for both polarities in Figure 11. Though observations are always more complex than model calculations, we find a surprisingly good agreement between observed and modelled elongation evolutions (*cf.* Figure 14). Models indicate a strong dependence of the elongation on the twist (the higher the twist, the more elongated the polarities are), and they also show that the elongation stays roughly the same until maximum flux is reached (*i.e.* when the entire cross-section of the

top of the flux rope has crossed the photosphere). Later on, the elongation of the tongues suddenly starts to decrease, *i.e.* both polarities are becoming more round-shaped. The most model-like elongation evolution is seen in AR 8011. The main difference with the model-curve is that the model does not include magnetic dispersal, *i.e.* there is no decrease of magnetic flux, while the decay phase could be followed in three out of the six cases (AR 8203, AR 8011, and AR 8015b).

In Figure 11 we indicate which of the two curves shows the elongation of the leading magnetic polarity. It is clear from the figure, that in all six cases the magnetic polarity leading in the sense of the solar rotation was more elongated than the following polarity. What can cause such asymmetry in the elongation of the leading and following polarity tongues?

There are other well-known asymmetries in emerging bipoles: (i) the leading sunspots are larger and longer-lived than following spots and (ii) in the divergent motions during emergence the leading sunspots move much faster westward than the following spots eastward. These asymmetries can be understood as being effects of the conservation of angular momentum as a flux rope is rising through the CZ, which makes the rising Ω-loop asymmetric, trailing the rotation, and induces a retrograde flow in the flux rope (from the leading towards the following leg), evacuating the former (*i.e.* increasing B in the leading leg) and increasing plasma pressure in the following leg, which leads to an expansion and consequent decrease of B there (Fan, Fisher, and Deluca, 1993; Moreno-Insertis, Caligari, and Schuessler, 1994; Caligari, Moreno-Insertis, and Schussler, 1995; Abbett, Fisher, and Fan, 2001). In the deformed flux rope the leading leg is more tilted to the vertical than the following leg, which can explain the observed asymmetries in sunspot motions, and that the PIL is closer to the centre-of-gravity of the following polarity than that of the leading one (van Driel-Gesztelyi and Petrovay, 1990). The higher magnetic field strength in the leading than that in the following leg of the Ω-loop makes the leading leg more buoyant than the following one, which further increases the asymmetry in sunspot motions, and explains recent findings by Tian and Alexander (2009) and Tian *et al.* (2011), who showed that magnetic helicity flux in ARs is systematically higher in the leading than in the following polarities.

The asymmetry in the elongation of the magnetic tongues, discovered by us, provides an independent confirmation of this asymmetric emerging flux rope model. If the leading leg of the emerging Ω-loop is more titled to the vertical than the following leg, the leading-polarity tongue will be more elongated than the following-polarity one. In the observed ARs the difference is significant, roughly a factor of three, implying significant eastward tilt of the emerging flux rope. 3-D spherical shell inelastic MHD simulations of the buoyant rise of magnetic flux tubes through the convection zone by Fan (2008) showed a deformation of the rising flux rope in the opposite sense (*i.e.* westward), which does not appear to be consistent with our findings. The observed asymmetry in the elongation of the magnetic tongues could perhaps be caused by stronger twist in the leading than that in the following leg of the emerging flux rope. However, the resulting torque would launch Alfvén waves, which would smooth the twist gradient, making this possibility less viable.

6. Conclusions

Longitudinal magnetograms provide only one component of the magnetic field. However, signatures of global magnetic twist can be inferred from the distribution of the longitudinal field during the emergence phase of bipolar ARs. The azimuthal (poloidal) magnetic field component of a flux rope has a projection in the longitudinal direction. This results in a characteristic elongated distribution pattern of the two polarities, called "magnetic tongues", sketched in Figure 1, which evolve as the flux rope is crossing the photosphere while the two polarities rotate around each other (Figure 2). This is only an apparent rotation, *i.e.* not linked to plasma or magnetic field motions. If the emerging flux tube is significantly twisted at its periphery, an emerging flux rope, with an east-west oriented axis, is first detected as an almost north-south bipole that later rotates progressively to the east-west direction, as the magnetic tongues first grow and then retract (see Figure 2).

MHD simulations of emerging twisted flux tubes also show a pattern of magnetic tongues at the photosphere, especially the recent MHD simulations which start with a curved flux tube below the photosphere (Hood *et al.*, 2009). The evolution of the tongues is similar in these simulations and in most observations; in particular, their retraction and the separation of the magnetic polarities indicate that most of the flux tube cross section has emerged above the photosphere. With less curved flux tubes in the MHD simulations, *e.g.* starting from a horizontal flux tube set more buoyant in some part along the axis, the magnetic tongues are more elongated. This is observed only in a subset of ARs, typically those that have large magnetic flux.

The spatial organization of the magnetic tongues lets us determine the sign of the twist by computing the acute angle from the bipole axis towards the PIL direction in the center of the AR. In most emerging flux tubes, the writhe helicity is much smaller than the twist helicity, so the tongues indicate the sign of the magnetic helicity injected in the corona (if significant writhe helicity is present, this is measured by the global rotation of the magnetic polarities, see López Fuentes *et al.*, 2003). In the present study we have verified that indeed the helicity sign inferred from the magnetic tongues is the same as the sign provided by other proxies, such as sheared or S-shaped coronal loops, relative shift of flare ribbons along the PIL, *in situ* magnetic field measurements in a magnetic cloud launched from the studied AR, and more directly with the results of magnetic helicity injection at the photospheric level. As a result, we confirm that magnetic tongues provide another reliable way to determine the magnetic helicity sign.

Still, as with other helicity proxies, there are limitations to the use of magnetic tongues. First, they can be unambigously identified only if the flux rope emerges in a relatively field-free environment (i.e. if the magnetic flux in the rope is well above the pre-existing background flux). Second, a single emergence of a flux rope is more favourable for a clear observation of magnetic tongues (this does not exclude the multi-emergences of small flux strands that form a single rope), unless the episodes of flux emergence are well separated in time (as in Figures 5 and 6). Finally, if the flux rope starts emerging at a few tens of degrees from the eastern solar limb, the full development, up to the retraction of the tongues, can

be followed in time for a typical AR having a magnetic flux around 10^{22} Mx. For much smaller bipoles, the full evolution from emergence to dispersion, can be observed in a few days, however (see *e.g.* Mandrini *et al.*, 2005).

The shape and the elongation or extension of the magnetic tongues depend both on the amount of the magnetic twist and its spatial distribution within the flux rope. However, the evolution of the tongues alone does not let us determine these parameters unambiguously, since the unknown geometry of the emerging flux rope is also involved. For example, even for a simple toroidal flux tube, as analytically described in the Appendix A, the elongation of the tongues depends on the radius of curvature of the flux rope axis (Figure 14). Moreover, MHD simulations show that the magnetic flux first accumulates below the photosphere, before the magnetic buoyancy instability takes effect at several small-scale parts of the rope. Then, the flux rope is strongly compressed in the vertical direction, it gets fragmented into flux tube strands and moreover reconnection occurs between these flux strands. All these processes imply that the geometry of the emerging field is *a priori* not known, so that the shape and extension of the magnetic tongues cannot be transformed directly to a twist profile. Still, in some ARs the appearance of tongues is delayed compared to the magnetic flux increase. These cases may be understood if the rope is much less twisted at the flux tube periphery than at its core. MHD simulations are needed to check wether or not a variable twist profile is the most plausible explanation (compared to a geometrical effect such as the distortion of the flux rope axis).

Analysing the evolution of the elongation magnetic tongues in six observed cases, we discovered a well-marked asymmetry between the leading and following polarities: the elongation of leading polarity tongues is systematically higher than that of the following polarity tongues. This asymmetry can be understood if the emerging Ω-loop is asymmetric, tilted eastward trailing the rotation. Such tilt can be attributed to the conservation of angular momentum during the rise of the flux rope through the CZ, a model successfully invoked to explain other well-known asymmetries in the stability and proper motions of leading and following magnetic polarities and the asymmetric location of the PIL (van Driel-Gesztelyi and Petrovay, 1990).

MHD simulations typically show that a flux rope suffers internal magnetic reconnection as it crosses the photosphere, so that the twisted flux tube later present in the corona is a subset of the initial one (Hood *et al.*, 2009). Still, the distribution of the vertical field component at the photosphere retains the signature of the twist of the initial flux tube. At some point of the MHD evolution, the coronal flux rope becomes unstable and gets ejected from the Sun in form of a CME. Following the eruption, an unbalance in the magnetic torque between the CZ and the coronal flux rope is expected to launch torsional Alfvén waves which will replenish the AR corona with magnetic helicity carried away by the CME (Longcope and Welsch, 2000). After that, photospheric magnetic diffusion and reconnection at the PIL forms a new flux rope that becomes unstable, (Aulanier *et al.*, 2010), leading to coronal helicity decrease followed by replenishment. This multiple-step process, of a progressive transfer of the magnetic helicity from the CZ to the interplanetary space, is evidenced by examples in which a large number of CMEs ($\approx$ 30-60) are launched during the full lifetime of an AR

(with flux $\approx 10^{22}$ Mx, Démoulin *et al.*, 2002, Green *et al.*, 2002, Mandrini *et al.*, 2004). The flux rope involved in one CME represents only a small fraction of the original rope which crossed the CZ, but it carries away part of the twist brought up by the flux rope. Then, unless subsequent flux emergences would create a mixed-helicity AR, the sign of the carried-away helicity will be the same as determined from the distribution of the longitudinal magnetic fields during the emergence of the flux rope, *i.e.* from the magnetic tongues. The ease of helicity sign determination using the widest-available longitudinal magnetograms makes magnetic tongues a valuable space weather tool.

Acknowledgements We thank E. Pariat for his helpful comments on the manuscript. The authors acknowledge financial support from ECOS-Sud (France) and MINCyT (Argentina) through their cooperative science program (N^o A08U01). CHM and MLL thank finantial support from the Argentinean grants UBACyT X127, PICT 2007/1790 (ANPCyT), and PIP 2009/0766 (CONICET). LvDG acknowledges funding through the Hungarian Science Foundation grant OTKA K81421, and the European Communitys FP7/2007 2013 programme through the SOTERIA Network (EU FP7 Space Science Project No. 218816). CHM is a member of the Carrera del Investigador Científico (CONICET). EIT and MDI data are a courtesy of SOHO/-EIT and SOHO/MDI consortia. SOHO is a project of international cooperation between ESA and NASA. Yohkoh is a mission of the Japanese Institute for Space and Astronautical Science.

Appendix

A. A Basic Twisted Flux Tube Model

We present below a simple model in order to describe the main properties of magnetic tongues as an Ω-shaped twisted flux tube emerges. The flux-tube shape is half a torus, with a main radius R and a small radius ρ (Figure 12). The torus center is located at the height $z = -d$ below the photosphere located at $z = 0$. A magnetic field line is described, in Cartesian coordinates, $\{x, y, z\}$ by

$$\mathbf{OM} = \{(R + \rho\cos\theta)\cos\phi,\ \rho\sin\theta,\ (R + \rho\cos\theta)\sin\phi - d\}\,, \tag{1}$$

where ϕ defines the location along the flux tube axis, and θ defines the rotation angle around the flux tube axis (Figure 12). We take a uniform twist along the flux rope, so these two angles are related by

$$\theta = 2N_{\rm t}\phi + \theta_0\,. \tag{2}$$

where θ_0 is a constant (θ value for $\phi = 0$) and $N_{\rm t}$ is the number of turns in half the torus.

Fields lines are tangent to the magnetic field $\mathbf{B}$, so $\mathbf{B}$ is parallel to the elementary difference d$\mathbf{OM}$. This implies that the azimuthal component, B_θ, is related to the axial component, B_ϕ by

$$B_\theta = 2N_{\rm t}\rho\, B_\phi/(R + \rho\cos\theta)\,. \tag{3}$$

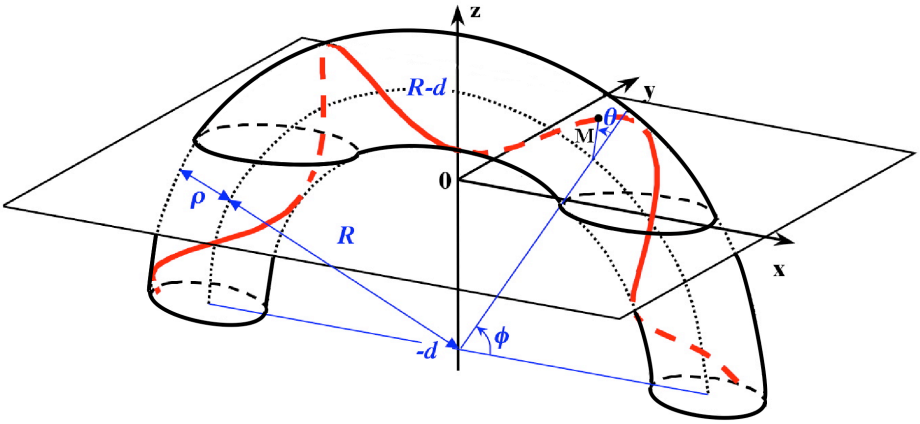

Figure 12. Sketch of a twisted flux tube having a half-torus shape. The red line is an example of a magnetic field line (with positive twist). The photospheric level is set at $z = 0$.

The condition $\nabla \cdot \mathbf{B} = 0$ and a uniform flux-rope cross section ($B_\rho = 0$), implies that $N_\mathrm{t} B_\phi$ is only a function of ρ.

Equations (1–3) define a simple flux rope which can be rewritten in the Cartesian coordinates x, y, z. In particular at the height $z = 0$, the vertical magnetic field component is

$$B_z(x, y) = (x - 2N_\mathrm{t}\, d\, y/u)\, B_\phi/u\,, \tag{4}$$

with $u = \sqrt{x^2 + d^2}$. As d decreases from $d \approx R + a$ to $d \approx 0$, $B_z(x, y)$ describes the evolution of a theoretical magnetogram where a twisted Ω-shaped flux tube is emerging. In order to keep the example the simplest possible, we do not consider the force balance and the flux rope is simply supposed to emerge without deformation up to $z = 0$ (we do not analyze the coronal part $z > 0$).

For the illustrating figures, we consider a simple example of flux rope, as follows. Following previous studies (*e.g.*, Emonet and Moreno-Insertis, 1998) we define the axial field as

$$B_\phi = B_0 \exp(-(\rho/a)^2)\,, \tag{5}$$

where a is the typical small radius of the flux rope and B_0 is the field strength on the axis. We also consider a uniform twist (N_t independent of ρ).

B. Analysis of the Magnetic Tongues

We analyse below the characteristics of the magnetic tongues, and illustrate how the elongation of tongues evolves as a function of magnetic twist and flux.

B.1. Direction of the Polarity Inversion Line (PIL)

One characteristic of the magnetic tongues is the orientation of the PIL in the center of the bipole (Figure 13). As the flux rope is more twisted, the azimuthal

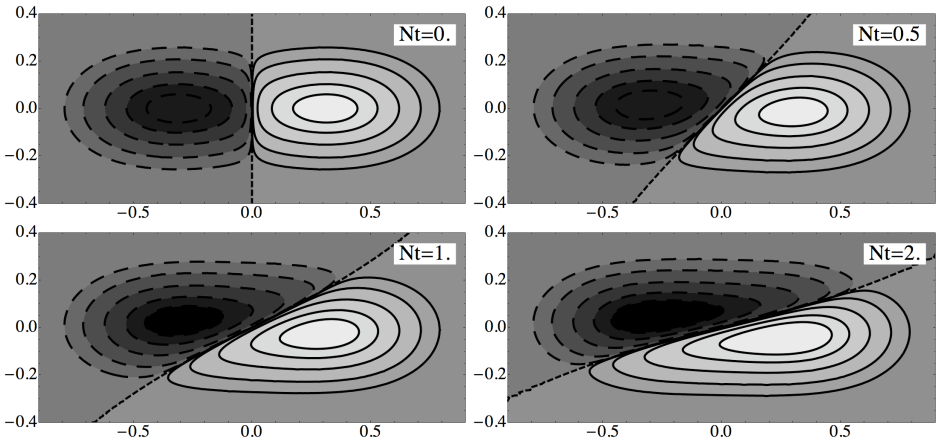

Figure 13. Orientation of the PIL for an east-west oriented torus with increasing twist (N_t) values. We plot the vertical magnetic field component at $z = 0$ for the model defined in Section A, with $d = R = 1$, $a/R = 0.1$ and for four different N_t values with uniformly distributed twist. The isocontour values are $(0.3, 3, 20, 80, 160, 320) \times 10^{-3} B_0$.

field component is larger, so the PIL is generally expected to be oriented closer to the bipole direction. Indeed, from Equation (4), the PIL equation is $x \approx 2N_\mathrm{t} y$ for $x \ll d$. Then, the angle δ_IL of the PIL with the x-axis is simply

$$\delta_\mathrm{IL} = \arctan(1/(2N_\mathrm{t}))\,. \tag{6}$$

It implies that the PIL shape, for $x \ll d$, is defined by the twist profile $N_\mathrm{t}(\rho)$. Then, the evolution of the PIL shape in the central part of an emerging AR provides a qualitative information on the twist profile. With a uniform twist profile the PIL is locally straight, and δ_IL is constant during the emerging process. The PIL is also more inclined in the x-direction (bipole direction) as the twist N_t is increasing (Figure 13). However, from observations, it is difficult to provide a quantitative estimate of the amount of twist present in the emerged part of the flux rope from the observed orientation of the PIL, as follows. At best, only the top part of the flux rope could be approximated by part of a torus, so δ_IL provides an estimation of $2N_\mathrm{t} = T\,R_c$ where T and R_c are the local twist angle per unit length and the curvature radius, respectively. R_c is not measurable from magnetograms and moreover it is expected to evolve during the emerging process so the twist present in the emerged part cannot be estimated. We conclude that following δ_IL during the emergence of an AR provides only a qualitative description of the twist profile, while the sign of δ_IL does provide the sign of the magnetic helicity (when the magnetic tongues are not masked by magnetic flux from another flux emergence.

B.2. Elongation of the Magnetic Tongues

Next, we analyse the shape of the magnetic tongues. In order to have robust quantities, we rely only on integrals computed from the analyzed magnetogram.

The mean position of the magnetic polarities is given by

$$\overline{x}_{\pm} = \frac{1}{F_{\pm}} \iint_{\pm B_z>0} x\,|B_z|\,\mathrm{d}x\,\mathrm{d}y\,; \quad \overline{y}_{\pm} = \frac{1}{F_{\pm}} \iint_{\pm B_z>0} y\,|B_z|\,\mathrm{d}x\,\mathrm{d}y\,, \tag{7}$$

where $\pm$ represents the positive or negative polarity. $F_{\pm}$ is the magnetic flux of the polarities

$$F_{\pm} = \iint_{\pm B_z>0} |B_z|\,\mathrm{d}x\,\mathrm{d}y\,. \tag{8}$$

The size of the AR is defined by

$$S_{\mathrm{AR}} = \sqrt{(\overline{x}_+ - \overline{x}_-)^2 + (\overline{y}_+ - \overline{y}_-)^2}\,. \tag{9}$$

The magnetic tongues are characterised by elongated magnetic polarities. We define the size, $S_{\pm}$, of the magnetic polarity $\pm$ in a direction making an angle φ with the x axis as

$$S^2_{\pm}(\varphi) = \frac{1}{F_{\pm}} \iint_{\pm B_z>0} \left[(x-\overline{x}_{\pm})\cos\varphi + (y-\overline{y}_{\pm})\sin\varphi\right]^2 |B_z|\,\mathrm{d}x\,\mathrm{d}y\,, \tag{10}$$

The expression between brackets inside the integral is the distance to the polarity center computed in the φ-direction. Equation (10) sums up the square of this distance, weighted by the vertical field strength, and normalised by the magnetic flux. $S_{\pm}$ is maximum in the direction φ_p defined by

$$\varphi_p = 0.5 \arctan[\,2\overline{xy}_{\pm}/(\overline{x^2}_{\pm} - \overline{y^2}_{\pm})\,]\,, \tag{11}$$

where the right hand side terms are defined by

$$\overline{x^i y^j}_{\pm} = \frac{1}{F_{\pm}} \iint_{\pm B_z>0} (x-\overline{x}_{\pm})^i (y-\overline{y}_{\pm})^j\,|B_z|\,\mathrm{d}x\,\mathrm{d}y\,, \tag{12}$$

and i, j are integers between 0 and 2. The maximum size of the polarity, $S_{\pm,\max}$, is

$$S^2_{\pm,\max} = S^2_{\pm}(\varphi_p) = \frac{1}{2}\left(\overline{x^2}_{\pm} + \overline{y^2}_{\pm} + \sqrt{(\overline{x^2}_{\pm} - \overline{y^2}_{\pm})^2 + 4\overline{xy}^2_{\pm}}\right)\,, \tag{13}$$

while the minimum size, $S_{\pm,\min}$, is obtained in an orthogonal direction ($\varphi_p + \pi/2$), and its value is obtained by replacing the + by a − sign in front of the square root in Equation (13). We define the relative elongation of the magnetic tongue, $S_{\pm,\mathrm{tongue}}$, by normalising with the AR size the difference of the sizes, so as

$$E_{\pm,\mathrm{tongue}} = (S_{\pm,\max} - S_{\pm,\min})/S_{\mathrm{AR}}\,. \tag{14}$$

The subtraction at the numerator implies that $E_{\pm,\mathrm{tongue}} = 0$ when the magnetic polarity is round.

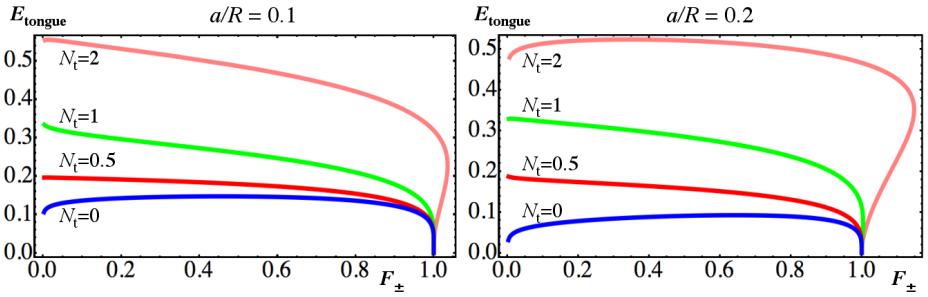

Figure 14. Evolution of the relative elongation of the magnetic tongue, $E_{\rm tongue}$ (Equation (14)) in function of the $B_z > 0$ magnetic flux normalised to the axial magnetic flux for the model defined in Section A.

B.3. Results with a Flux Rope Model

We next apply the above analysis to the model defined in Section A. The orientation of the tongues, defined by φ_p, has a non-monotonous dependance on $N_{\rm t}$, and it is typically small (around 10^0) for low aspect ratio values (*e.g.* $a/R \approx 0.1$). Then, φ_p does not characterise well the magnetic tongues.

A better characterisation is given by $E_{\pm,\rm tongue}$ since it has a monotonic and important variation with $N_{\rm t}$ (Figure 14). In these plots the flux-rope's upper part starts to cross $z = 0$ on the left side of the panel, and the half torus is located above $z = 0$ on the right side (where $F_z = 1$, and $E_{\pm,\rm tongue} = 0$). The typical evolution of a theoretical magnetogram, with the flux rope defined in Section A, is given in Figure 2. For large values of $N_{\rm t}$, F_z is going above unity due to the important contribution of the azimuthal field component to B_z. With the selected uniform distribution of $N_{\rm t}$ in the flux-rope cross section, $E_{\pm,\rm tongue}$ has a weak variation during most of the flux-rope emergence. $E_{\pm,\rm tongue}$ is also slightly affected by a/R for values typical of ARs.

References

Abbett, W.P., Fisher, G.H., Fan, Y.: 2001, The effects of rotation on the evolution of rising omega loops in a stratified model convection zone. *Astrophys. J.* **546**, 1194 – 1203. doi:10.1086/318320.

Archontis, V., Hood, A.W.: 2010, Flux emergence and coronal eruption. *Astron. Astrophys.* **514**, A56. doi:10.1051/0004-6361/200913502.

Archontis, V., Moreno-Insertis, F., Galsgaard, K., Hood, A., O'Shea, E.: 2004, Emergence of magnetic flux from the convection zone into the corona. *Astron. Astrophys.* **426**, 1047 – 1063. doi:10.1051/0004-6361:20035934.

Archontis, V., Hood, A.W., Savcheva, A., Golub, L., Deluca, E.: 2009, On the structure and evolution of complexity in sigmoids: a flux emergence model. *Astrophys. J.* **691**, 1276 – 1291. doi:10.1088/0004-637X/691/2/1276.

Asai, A., Shibata, K., Ishii, T.T., Oka, M., Kataoka, R., Fujiki, K., Gopalswamy, N.: 2009, Evolution of the anemone AR NOAA 10798 and the related geo-effective flares and CMEs. *J. Geophys. Res.* **114**, A00A21. doi:10.1029/2008JA013291.

Attrill, G.D.R., Harra, L.K., van Driel-Gesztelyi, L., Démoulin, P.: 2007, Coronal "wave": magnetic footprint of a coronal mass ejection? *Astrophys. J. Lett.* **656**, 101 – 104. doi:10.1086/512854.

Aulanier, G., Török, T., Démoulin, P., DeLuca, E.E.: 2010, Formation of torus-unstable flux ropes and electric currents in erupting sigmoids. *Astrophys. J.* **708**, 314 – 333. doi:10.1088/0004-637X/708/1/314.

Berdichevsky, D.B., Farrugia, C.J., Thompson, B.J., Lepping, R.P., Reames, D.V., Kaiser, M.L., Steinberg, J.T., Plunkett, S.P., Michels, D.J.: 2002, Halo-coronal mass ejections near the 23rd solar minimum: lift-off, inner heliosphere, and in situ (1 AU) signatures. *Ann Geophys.* **20**, 891 – 916. doi:10.5194/angeo-20-891-2002.

Burnette, A.B., Canfield, R.C., Pevtsov, A.A.: 2004, Photospheric and coronal currents in solar active regions. *Astrophys. J.* **606**, 565 – 570. doi:10.1086/382775.

Caligari, P., Moreno-Insertis, F., Schussler, M.: 1995, Emerging flux tubes in the solar convection zone. 1: Asymmetry, tilt, and emergence latitude. *Astrophys. J.* **441**, 886 – 902. doi:10.1086/175410.

Canfield, R.C., Hudson, H.S., McKenzie, D.E.: 1999, Sigmoidal morphology and eruptive solar activity. *Geophys. Res. Lett.* **26**, 627 – 630. doi:10.1029/1999GL900105.

Canou, A., Amari, T., Bommier, V., Schmieder, B., Aulanier, G., Li, H.: 2009, Evidence for a pre-eruptive twisted flux rope using the THEMIS vector magnetograph. *Astrophys. J. Lett.* **693**, 27 – 30. doi:10.1088/0004-637X/693/1/L27.

Chae, J.: 2001, Observational determination of the rate of magnetic helicity transport through the solar surface via the horizontal motion of field line footpoints. *Astrophys. J. Lett.* **560**, 95 – 98. doi:10.1086/324173.

Chae, J., Moon, Y.J., Park, Y.D.: 2004, Determination of magnetic helicity content of solar active regions from SOHO/MDI magnetograms. *Solar Phys.* **223**, 39 – 55. doi:10.1007/s11207-004-0938-9.

Chandra, R., Schmieder, B., Aulanier, G., Malherbe, J.M.: 2009, Evidence of magnetic helicity in emerging flux and associated flare. *Solar Phys.* **258**, 53 – 67. doi:10.1007/s11207-009-9392-z.

Chandra, R., Pariat, E., Schmieder, B., Mandrini, C.H., Uddin, W.: 2010, How can a negative magnetic helicity active region generate a positive helicity magnetic cloud? *Solar Phys.* **261**, 127 – 148. doi:10.1007/s11207-009-9470-2.

Cheung, M., Schüssler, M., Moreno-Insertis, F.: 2005, 3D magneto-convection and flux emergence in the photosphere. In: Innes, D.E., Lagg, A., Solanki, S.A. (eds.) *Chromospheric and Coronal Magnetic Fields, ESA SP-596*, paper 54.1 (on CDROM).

Cheung, M.C.M., Moreno-Insertis, F., Schüssler, M.: 2006, Moving magnetic tubes: fragmentation, vortex streets and the limit of the approximation of thin flux tubes. *Astron. Astrophys.* **451**, 303 – 317. doi:10.1051/0004-6361:20054499.

Cheung, M.C.M., Schüssler, M., Tarbell, T.D., Title, A.M.: 2008, Solar surface emerging flux regions: A comparative study of radiative MHD modeling and Hinode SOT observations. *Astrophys. J.* **687**, 1373 – 1387. doi:10.1086/591245.

Cristiani, G., Martinez, G., Mandrini, C.H., Giménez de Castro, C.G., da Silva, C.W., Rovira, M.G., Kaufmann, P.: 2007, Spatial characterization of a flare using radio observations and magnetic field topology. *Solar Phys.* **240**, 271 – 281. doi:10.1007/s11207-006-0337-5.

Cristiani, G., Giménez de Castro, C.G., Mandrini, C.H., Machado, M.E., Silva, I.D.B.E., Kaufmann, P., Rovira, M.G.: 2008, A solar burst with a spectral component observed only above 100 GHz during an M class flare. *Astron. Astrophys.* **492**, 215 – 222. doi:10.1051/0004-6361:200810367.

Delaboudiniére, J.-P., Artzner, G.E., Brunaud, J., Gabriel, A.H., Hochedez, J.F., Millier, F., *et al.*: 1995, EIT: Extreme-ultraviolet imaging telescope for the SOHO mission. *Solar Phys.* **162**, 291 – 312. doi:10.1007/BF00733432.

Démoulin, P., Pariat, E.: 2009, Modelling and observations of photospheric magnetic helicity. *Adv. Space Res.* **43**, 1013 – 1031. doi:10.1016/j.asr.2008.12.004.

Démoulin, P., Priest, E.R., Lonie, D.P.: 1996, Three-dimensional magnetic reconnection without null points 2. Application to twisted flux tubes. *J. Geophys. Res.* **101** (A10), 7631 – 7646. doi:10.1029/95JA03558.

Démoulin, P., Mandrini, C.H., van Driel-Gesztelyi, L., Thompson, B.J., Plunkett, S., Kovári, Z., Aulanier, G., Young, A.: 2002, What is the source of the magnetic helicity shed by CMEs? The long-term helicity budget of AR 7978. *Astron. Astrophys.* **382**, 650 – 665. doi:10.1051/0004-6361:20011634.

Emonet, T., Moreno-Insertis, F.: 1998, The physics of twisted magnetic tubes rising in a stratified medium: two-dimensional results. *Astrophys. J.* **492**, 804 – 821. doi:10.1086/305074.

Fan, Y.: 2008, The three-dimensional evolution of buoyant magnetic flux tubes in a model solar convective envelope. *Astrophys. J.* **676**, 680 – 697. doi:10.1086/527317.

Fan, Y.: 2009, The emergence of a twisted flux tube into the solar atmosphere: sunspot rotations and the formation of a coronal flux rope. *Astrophys. J.* **697**, 1529 – 1542. doi:10.1088/0004-637X/697/2/1529.

Fan, Y., Fisher, G.H., Deluca, E.E.: 1993, The origin of morphological asymmetries in bipolar active regions. *Astrophys. J.* **405**, 390 – 401. doi:10.1086/172370.

Georgoulis, M.K., LaBonte, B.J.: 2006, Reconstruction of an inductive velocity field vector from Doppler motions and a pair of solar vector magnetograms. *Astrophys. J.* **636**, 475 – 495. doi:10.1086/497978.

Gibson, S.E., Fan, Y., Mandrini, C., Fisher, G., Démoulin, P.: 2004, Observational consequences of a magnetic flux rope emerging into the corona. *Astrophys. J.* **617**, 600 – 613. doi:10.1086/425294.

Glover, A., Ranns, N.D.R., Harra, L.K., Culhane, J.L.: 2000, The onset and association of CMEs with sigmoidal active regions. *Geophys. Res. Lett.* **27**, 2161 – 2164. doi:10.1029/2000GL000018.

Gopalswamy, N., Kaiser, M.L., Sato, J., Pick, M.: 2000, Shock wave and EUV transient during a flare. In: Ramaty, R., Mandzhavidze, N. (eds.) (ed.) *High Energy Solar Physics Workshop - Anticipating HESSI*, *ASP Conf. Ser.* **206**, 351 – 354.

Green, L.M., Kliem, B.: 2009, Flux rope formation preceding coronal mass ejection onset. *Astrophys. J. Lett.* **700**, 83 – 87. doi:10.1088/0004-637X/700/2/L83.

Green, L.M., López fuentes, M.C., Mandrini, C.H., Démoulin, P., Van Driel-Gesztelyi, L., Culhane, J.L.: 2002, The magnetic helicity budget of a CME-prolific active region. *Solar Phys.* **208**, 43 – 68. doi:10.1023/A:1019658520033.

Green, L.M., Kliem, B., Török, T., van Driel-Gesztelyi, L., Attrill, G.D.R.: 2007, Transient coronal sigmoids and rotating erupting flux ropes. *Solar Phys.* **246**, 365 – 391. doi:10.1007/s11207-007-9061-z.

Hood, A.W., Archontis, V., Galsgaard, K., Moreno-Insertis, F.: 2009, The emergence of toroidal flux tubes from beneath the solar photosphere. *Astron. Astrophys.* **503**, 999 – 1011. doi:10.1051/0004-6361/200912189.

Jeong, H., Chae, J.: 2007, Magnetic helicity injection in active regions. *Astrophys. J.* **671**, 1022 – 1033. doi:10.1086/522666.

Jouve, L., Brun, A.S.: 2009, Three-dimensional nonlinear evolution of a magnetic flux tube in a spherical shell: Influence of turbulent convection and associated mean flows. *Astrophys. J.* **701**, 1300 – 1322. doi:10.1088/0004-637X/701/2/1300.

LaBonte, B.J., Georgoulis, M.K., Rust, D.M.: 2007, Survey of magnetic helicity injection in regions producing X-class flares. *Astrophys. J.* **671**, 955 – 963. doi:10.1086/522682.

Leamon, R.J., Canfield, R.C., Pevtsov, A.A.: 2002, Properties of magnetic clouds and geomagnetic storms associated with eruption of coronal sigmoids. *J. Geophys. Res.* **107**(A9), 1234. doi:10.1029/2001JA000313.

Li, H., Schmieder, B., Song, M.T., Bommier, V.: 2007, Interaction of magnetic field systems leading to an X1.7 flare due to large-scale flux tube emergence. *Astron. Astrophys.* **475**, 1081 – 1091. doi:10.1051/0004-6361:20077500.

Liu, J., Zhang, H.: 2006, The magnetic field, horizontal motion and helicity in a fast emerging flux region which eventually forms a delta spot. *Solar Phys.* **234**, 21 – 40. doi:10.1007/s11207-006-2091-0.

Liu, J., Zhang, Y., Zhang, H.: 2008, Relationship between powerful flares and dynamic evolution of the magnetic field at the solar surface. *Solar Phys.* **248**, 67 – 84. doi:10.1007/s11207-008-9149-0.

Longcope, D.W., Welsch, B.T.: 2000, A model for the emergence of a twisted magnetic flux tube. *Astrophys. J.* **545**, 1089 – 1100. doi:10.1086/317846.

López Fuentes, M.C., Démoulin, P., Mandrini, C.H., van Driel-Gesztelyi, L.: 2000, The counterkink rotation of a non-Hale active region. *Astrophys. J.* **544**, 540 – 549. doi:10.1086/317180.

López Fuentes, M.C., Démoulin, P., Mandrini, C.H., Pevtsov, A.A., van Driel-Gesztelyi, L.: 2003, Magnetic twist and writhe of active regions. On the origin of deformed flux tubes. *Astron. Astrophys.* **397**, 305 – 318. doi:10.1051/0004-6361:20021487.

Luoni, M.L., Mandrini, C.H., Dasso, S., Démoulin, P., Van Driel-Gesztelyi, L.: 2007, From the photosphere to the interplanetary medium: The magnetic helicity sign from observations. *Boletin Asoc. Arg. Astron.* **50**, 43 – 46.

MacTaggart, D., Hood, A.W.: 2009, On the emergence of toroidal flux tubes: general dynamics and comparisons with the cylinder model. *Astron. Astrophys.* **507**, 995 – 1004. doi:10.1051/0004-6361/200912930.

Magara, T.: 2001, Dynamics of emerging flux tubes in the Sun. *Astrophys. J.* **549**, 608 – 628. doi:10.1086/319073.

Magara, T.: 2004, A model for dynamic evolution of emerging magnetic fields in the Sun. *Astrophys. J.* **605**, 480 – 492. doi:10.1086/382148.

Magara, T., Longcope, D.W.: 2003, Injection of magnetic energy and magnetic helicity into the solar atmosphere by an emerging magnetic flux tube. *Astrophys. J.* **586**, 630 – 649. doi:10.1086/367611.

Manchester, W. IV, Gombosi, T., DeZeeuw, D., Fan, Y.: 2004, Eruption of a buoyantly emerging magnetic flux rope. *Astrophys. J.* **610**, 588 – 596. doi:10.1086/421516.

Mandrini, C.H., Démoulin, P., van Driel-Gesztelyi, L., Green, L., López Fuentes, M.C.: 2004, Magnetic helicity budget of solar-active regions from the photosphere to magnetic clouds. *Astrophys. Space Sci.* **290**, 319 – 344. doi:10.1023/B:ASTR.0000032533.31817.0e.

Mandrini, C.H., Pohjolainen, S., Dasso, S., Green, L.M., Démoulin, P., van Driel-Gesztelyi, L., Copperwheat, C., Foley, C.: 2005, Interplanetary flux rope ejected from an X-ray bright point. The smallest magnetic cloud source-region ever observed. *Astron. Astrophys.* **434**, 725 – 740. doi:10.1051/0004-6361:20041079.

Moore, R.L., Sterling, A.C., Hudson, H.S., Lemen, J.R.: 2001, Onset of the magnetic explosion in solar flares and coronal mass ejections. *Astrophys. J.* **552**, 833 – 848. doi:10.1086/320559.

Moreno-Insertis, F., Caligari, P., Schuessler, M.: 1994, Active region asymmetry as a result of the rise of magnetic flux tubes. *Solar Phys.* **153**, 449 – 452. doi:10.1007/BF00712518.

Murray, M.J., Hood, A.W.: 2008, Emerging flux tubes from the solar interior into the atmosphere: effects of non-constant twist. *Astron. Astrophys.* **479**, 567 – 577. doi:10.1051/0004-6361:20078852.

Murray, M.J., Hood, A.W., Moreno-Insertis, F., Galsgaard, K., Archontis, V.: 2006, 3D simulations identifying the effects of varying the twist and field strength of an emerging flux tube. *Astron. Astrophys.* **460**, 909 – 923. doi:10.1051/0004-6361:20065950.

Nindos, A., Zhang, J., Zhang, H.: 2003, The magnetic helicity budget of solar active regions and coronal mass ejections. *Astrophys. J.* **594**, 1033 – 1048. doi:10.1086/377126.

Pariat, E., Démoulin, P., Berger, M.A.: 2005, Photospheric flux density of magnetic helicity. *Astron. Astrophys.* **439**, 1191 – 1203. doi:10.1051/0004-6361:20052663.

Pariat, E., Aulanier, G., Schmieder, B., Georgoulis, M.K., Rust, D.M., Bernasconi, P.N.: 2004, Resistive emergence of undulatory flux tubes. *Astrophys. J.* **614**, 1099 – 1112. doi:10.1086/423891.

Parker, E.N.: 1979, Sunspots and the physics of magnetic flux tubes. IX - Umbral dots and longitudinal overstability. *Astrophys. J.* **234**, 333 – 347. doi:10.1086/157501.

Pevtsov, A.A.: 2002, Sinuous coronal loops at the Sun. In: Martens, P.C.H., Cauffman, D. (eds.) *Multi-Wavelength Observations of Coronal Structure and Dynamics, COSPAR Colloq. Ser.* **13**, 125 – 134.

Pevtsov, A.A., Canfield, R.C., McClymont, A.N.: 1997, On the subphotospheric origin of coronal electric currents. *Astrophys. J.* **481**, 973 – 977. doi:10.1086/304065.

Rust, D.M., Kumar, A.: 1996, Evidence for helically kinked magnetic flux ropes in solar eruptions. *Astrophys. J. Lett.* **464**, 199 – 203. doi:10.1086/310118.

Scherrer, P.H., Bogart, R.S., Bush, R.I., Hoeksema, J.T., Kosovichev, A.G., Schou, J., *et al.*: 1995, The solar oscillations investigation - Michelson doppler imager. *Solar Phys.* **162**, 129 – 188. doi:10.1007/BF00733429.

Strous, L.H., Scharmer, G., Tarbell, T.D., Title, A.M., Zwaan, C.: 1996, Phenomena in an emerging active region. I. Horizontal dynamics. *Astron. Astrophys.* **306**, 947 – 959.

Tian, L., Alexander, D.: 2006, Role of sunspot and sunspot-group rotation in driving sigmoidal active region eruptions. *Solar Phys.* **233**, 29 – 43. doi:10.1007/s11207-006-2505-z.

Tian, L., Alexander, D.: 2008, On the origin of magnetic helicity in the solar corona. *Astrophys. J.* **673**, 532 – 543. doi:10.1086/524129.

Tian, L., Alexander, D.: 2009, Asymmetry of helicity injection flux in emerging active regions. *Astrophys. J.* **695**, 1012 – 1023. doi:10.1088/0004-637X/695/2/1012.

Tian, L., Alexander, D., Nightingale, R.: 2008, Origins of coronal energy and helicity in NOAA 10030. *Astrophys. J.* **684**, 747 – 756. doi:10.1086/589492.

Tian, L., Liu, Y., Yang, J., Alexander, D.: 2005b, The role of the kink instability of a long-lived active region AR 9604. *Solar Phys.* **229**, 237 – 253. doi:10.1007/s11207-005-6884-3.

Tian, L., Démoulin, P., Alexander, D., Zhu, C.: 2011, On asymmetry of magnetic helicity in emerging active regions: High-resolution observations. *Astrophys. J.* **727**, 28. doi:10.1088/0004-637X/727/1/28.

Titov, V.S., Démoulin, P.: 1999, Basic topology of twisted magnetic configurations in solar flares. *Astron. Astrophys.* **351**, 707 – 720.

Tsuneta, S., Acton, L., Bruner, M., Lemen, J., Brown, W., Caravalho, R., *et al.*: 1991, The soft X-ray telescope for the SOLAR-A mission. *Solar Phys.* **136**, 37 – 67. doi:10.1007/BF00151694.

van Driel-Gesztelyi, L., Petrovay, K.: 1990, Asymmetric flux loops in active regions. *Solar Phys.* **126**, 285 – 298. doi:10.1007/BF00153051.

Wu, G.P., Huang, G.L., Tang, Y.H., Xu, A.A.: 2005, The observational evidence on the loop interaction in a flare CME event on April 15, 1998. *Solar Phys.* **227**, 327 – 337. doi:10.1007/s11207-005-2512-5.

Yamamoto, T.T., Kusano, K., Maeshiro, T., Yokoyama, T., Sakurai, T.: 2005, Magnetic helicity injection and sigmoidal coronal loops. *Astrophys. J.* **624**, 1072 – 1079. doi:10.1086/429363.

Yang, S., Büchner, J., Zhang, H.: 2009a, Magnetic helicity exchange between neighboring active regions. *Astrophys. J. Lett.* **695**, 25 – 30. doi:10.1088/0004-637X/695/1/L25.

Yang, S., Zhang, H., Büchner, J.: 2009b, Magnetic helicity accumulation and tilt angle evolution of newly emerging active regions. *Astron. Astrophys.* **502**, 333 – 340. doi:10.1051/0004-6361/200810032.

Zwaan, C.: 1985, The emergence of magnetic flux. *Solar Phys.* **100**, 397 – 414. doi:10.1007/BF00158438.